

# The Evolution of Impact Basins: Viscous Relaxation of Topographic Relief

SEAN C. SOLOMON AND ROBERT P. COMER

*Department of Earth and Planetary Sciences, Massachusetts Institute of Technology  
Cambridge, Massachusetts 02139*

JAMES W. HEAD

*Department of Geological Sciences, Brown University, Providence, Rhode Island 02912*

We evaluate the hypothesis that viscous relaxation has been an important process for modifying the topographic profiles of ancient large impact basins on the moon. We adopt a representative topographic profile of the Orientale basin, the youngest large impact basin on the moon, as an estimate of the initial topography of older basins of similar horizontal dimensions, and we predict the topographic profiles that would result from viscous relaxation according to a number of simple analytical representations of the rheological response of the moon to surface topography. At wavelengths greater than the thickness of a high-viscosity lithosphere, both a decrease in viscosity with depth and the partial to complete isostatic compensation of topographic relief have pronounced effects on the wavelength-dependent relaxation times and must be considered in modeling viscous relaxation for features as large as impact basins. The effect of a decrease in viscosity with depth is to enhance the rate of viscous relaxation at long wavelengths, while the rate of relaxation decreases substantially for the fraction of long-wavelength topography which is isostatically compensated as an initial condition. These models are applied to two pre-Nectarian basins on the moon, the Tranquillitatis basin on the lunar nearside and the much larger and older South Pole-Aitken basin on the farside. The topographic profile of Tranquillitatis, after correcting for the effect of mare basalt fill, is consistent with significant viscous relaxation of relief prior to the oldest episode of mare volcanism preserved as a surface unit. The large topographic relief of the larger farside basin, on the contrary, is not consistent with significant viscous relaxation and implies a mean crustal viscosity at least a factor of 10 higher than for the central nearside over the time interval during which substantial viscous relaxation of older nearside basins such as Tranquillitatis probably occurred. A difference in typical crustal temperature profiles between the farside and nearside is the most likely explanation of such a viscosity difference; such a nearside-farside asymmetry in near-surface temperature may date from the time of crust-mantle differentiation and may have persisted because of the different histories of late-stage impact basin formation and mare volcanism on the two hemispheres.

## INTRODUCTION

Impact basins are large, generally circular structures exceeding about 200 km in diameter and often displaying two or more concentric rings. Impact basins formed in the first billion years of planetary history; they can be seen on the surfaces of the moon, Mars, Mercury, and the Galilean satellites [Hartmann and Wood, 1971; Malin, 1976; Wood and Head, 1976; McKinnon and Melosh, 1980], and they may have been preserved on the surface of Venus [Schaber and Boyce, 1977]. Their presence on these bodies makes it a virtual certainty that such impact basins also formed on the early surface of the earth, though their formation was prior to the time when stable nuclei of continental lithosphere could persist unmodified to the present, so that these early terrestrial impact basins have not been preserved. The abundances of impact basins on the solid surfaces of the solar system indicate that basin formation was an important geological process in the early, formative years of planetary crustal evolution [Head and Solomon, 1981].

The formation of a basin concentrates a substantial amount of heat into a small area and volume near the surface of a planet [O'Keefe and Ahrens, 1977]. In addition, impact

basins become a focus for other planetary processes, such as volcanism and tectonic activity, long after the impact event. These volcanic and tectonic processes can modify the structure and morphology of the impact basin. The timing and character of such modification processes provide important information about the nature and evolution of the interior of a planet.

As part of an ongoing effort to understand the properties and processes that affect the formation and evolution of impact basins [Head and Solomon, 1981], we have identified three major processes that act to modify impact basins over geologically long time scales (millions to billions of years): (1) thermal contraction and thermal stress associated with the loss of heat from basin formation, (2) relaxation of topographic relief by viscous flow for basins formed in regions of elevated temperatures at shallow depth, and (3) volcanic filling and lithospheric loading. The last process and its effect on the volcanic and tectonic history of major impact basins on the moon and Mars have been treated at length [Solomon and Head, 1979, 1980; Solomon et al., 1979; Comer et al., 1979, 1980]. The first process and its influence on basin topography and tectonics are the topics of parallel studies [Bratt et al., 1981; Church et al., 1982]. The second process, viscous relaxation as a modifier of impact basin topography, is the subject of this paper.

While the rugged ring mountains of comparatively young basins are often strikingly evident on the present surfaces of

Copyright © 1982 by the American Geophysical Union.

Paper number 2B0227.  
0148-0227/82/002B-0227\$05.00



Fig. 1a. The Orientale basin on the moon. Portion of Lunar orbiter photograph LO IV-194M.

the moon, Mars, and Mercury (Figure 1), the ring structures of older basins on these planets are often incomplete and much more poorly preserved. There also are circular basins, possibly of impact origin, on Venus and on the icy Galilean satellites with at most very modest topographic relief. A major candidate for the process responsible for these different degrees of preservation of impact basin topography in the solar system is viscous relaxation of the stresses generated by topographic relief. The rate and degree of viscous relaxation is related to the regional thermal environment and to the thermal evolution of a planet. Extensive relaxation has probably occurred only in impact basins formed early

enough in the history of a planet so that near-surface temperatures were high and solid state creep could readily occur on the scale of basin dimensions.

A number of previous studies have supported the suggestion that viscous relaxation has been an important modification process for many impact craters and basins. Viscous relaxation has been proposed by several workers to explain both the reduced topographic relief in a number of specific lunar craters, particularly those with fractured and apparently uplifted floors [Masursky, 1964; Daneš, 1965; Scott, 1967; Baldwin, 1968; Pike, 1968], and the general reduction in lunar crater relief with age [Baldwin, 1971; Kunze, 1974]. It

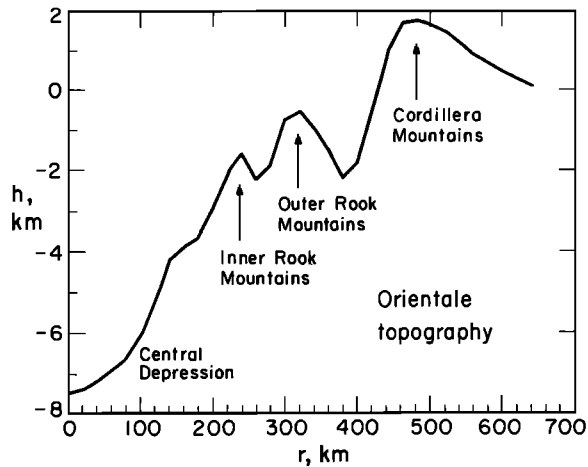


Fig. 1b. Representative topographic profile for the Orientale basin [Head *et al.*, 1981];  $h = 0$  corresponds to the typical level of surrounding terrain at a sufficient distance from the basin so that ejecta deposits are not a significant contributor to topography.

has recently been demonstrated that the topographic profiles of several lunar floor-fractured craters 15 to 40 km in diameter can be quantitatively matched by viscous relaxation of the topographic profile of a fresh crater of the same rim diameter [Hall *et al.*, 1981]. The lack of evidence from Bouguer gravity anomalies for the mantle uplift that would accompany viscous relaxation for four Imbrian-age craters 70 to 200 km in diameter, however, has been noted by Dvorak and Phillips [1978]. Viscous relaxation has been suggested to account for the very subdued topographic relief of ancient impact basins on Mercury [Schaber *et al.*, 1977] and of possible impact basins on Venus [Masursky *et al.*, 1980]. Clear evidence for viscous relaxation of craters is observable on Ganymede and Callisto [Smith *et al.*, 1979]. Quantitative models for viscous modification of craters on icy satellites have been constructed by Parmentier and Head [1981].

In this paper we use a representative topographic profile of the youngest large basin on the moon (Orientale) to explore the consequences of viscous relaxation of basin topography. We consider a range of simple analytical models for viscous flow, and we show that the wavelength-dependent time constants for viscous decay are sensitive to a decrease in viscosity with depth and to the extent of isostatic compensation of initial topography. Finally, we demonstrate that the present topographic profiles for comparatively older impact basins on at least the nearside of the moon are consistent with the hypothesis that viscous relaxation has been a substantial contributor to the modification of topography. The topographic relief preserved for a large ancient basin on the lunar farside suggests that crustal viscosities on the farside of the moon early in lunar history were at least an order of magnitude larger than contemporaneous viscosities on the nearside.

#### ORIENTALE BASIN TOPOGRAPHY

The Orientale basin on the moon is perhaps the best preserved large impact basin in the inner solar system. In plan view (Figure 1a), the basin is outlined by the Cordillera Mountains, which form a ring approximately 900 km in diameter [Head, 1974; Moore *et al.*, 1974; Howard *et al.*,

1974]. Concentric to this outer ring are the outer Rook Mountains (620 km in diameter), the inner Rook Mountains (480 km in diameter), and an inner depression (approximately 320 km in diameter), which is partially filled with mare material. The rim of the original impact crater cavity, according to the arguments of Head [1974], corresponds approximately to the outer Rook Mountain ring. By this argument, the Cordillera ring is a huge fault scarp that formed during the terminal stages of the cratering event by inward collapse of an annulus of lithosphere surrounding the transient crater cavity [Head, 1974; Melosh and McKinnon, 1978]. The inner Rook Mountains correspond to a central peak ring within the crater.

The interior topography of the eastern half of the Orientale basin has been determined by Head *et al.* [1981] from a compilation of limb-height measurements. A characteristic profile from the center of the basin to beyond the Cordillera Mountain ring is shown in Figure 1b. The central floor of the basin lies at about 9 km below the peaks of the outer ring and at about 7.5 km below the level of the surrounding lunar terrain. The three prominent concentric ring mountains display local relief of 1–3 km. The central depression within the inner Rook Mountain ring has 3–4 km of local relief.

Several factors may influence the initial topography of impact basins of a given size. Melosh and McKinnon [1978] have proposed that cavity collapse and ring formation are related to lithospheric thickness. If the cavity depth exceeds the effective elastic thickness of the lithosphere (at the large strain rates of impact basin formation), then sublithospheric flow enhances cavity collapse and can lead to formation of the outer basin ring. If cavity depth is less than lithospheric thickness, ring formation and cavity collapse are inhibited. Ring formation and cavity collapse may therefore be favored early in lunar history when the elastic lithosphere is likely to have been relatively thin [Head and Solomon, 1980]. Further, several processes in addition to viscous flow may modify the initial topography of a basin, including impact degradation, local thermal contraction, and volcanic flooding.

We adopt the present topographic profile of Orientale as a model for the original topography of older lunar basins of similar horizontal dimensions. The well-developed ring structure around Orientale suggests that cavity collapse has taken place. In addition, Orientale is the youngest large lunar basin [Hartmann and Wood, 1971; Wilhelms, 1979], so that it has not been modified by the emplacement of ejecta deposits from any younger basins and the volume of mare basalt fill within the basin is thought to be relatively small [Head, 1974]. Abundant Orientale basin interior deposits interpreted as mixtures of shock-melted material and partially melted to unmelted ejecta show no evidence for major structural deformation [Head, 1974]. Thus any major structural adjustments to basin topographic relief related to collapse of the transient cavity must have been completed prior to final cooling of these impact melt deposits [Head, 1974]. Some early topographic modifications, occurring subsequent to impact melt emplacement and related to local thermal contraction [Bratt *et al.*, 1981; Church *et al.*, 1982], may have increased the depth of the inner depression. Any geologically long-term isostatic or viscous adjustments to the early basin structure, however, must have been quite modest. The Orientale basin appears to have formed sufficiently late in lunar history so that the crust and lithosphere were charac-

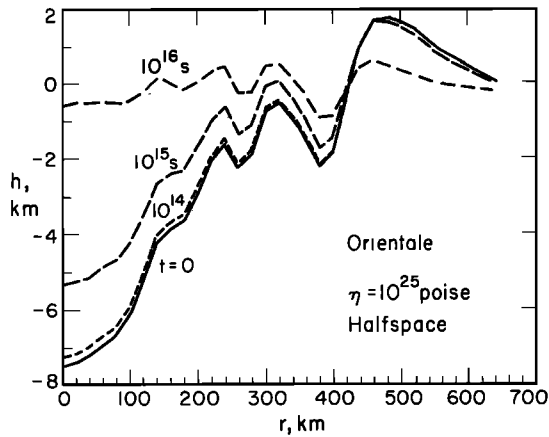


Fig. 2. Viscous relaxation of Orientale basin topography for a half-space model for lunar rheology. Profiles are shown at  $t = 0$ ,  $10^{14}$  s (3 m.y.),  $10^{15}$  s (30 m.y.), and  $10^{16}$  s (300 m.y.); these times scale linearly with the assumed viscosity, here taken as  $\eta = 10^{25}$  P.

terized by temperatures low enough to resist viscous flow and to permit the long-term support of basin topography by finite strength.

#### VISCOUS RELAXATION

##### Half-Space Model

With the topographic profile of Orientale as an assumed initial state, we now examine the effect of viscous relaxation on the topography of basins formed earlier in lunar history when near-surface temperatures were high and solid state creep was a significant process at shallow depths and on relatively short geological time scales [e.g., Solomon *et al.*, 1981]. We consider a range of simple models for the response of the moon to initial basin topographic relief; in all of these models the response is determined analytically so that we may understand the effect of important parameters on the relaxation process.

The simplest model for lunar rheology is a half space of uniform Newtonian viscosity  $\eta$ , uniform density  $\rho$ , and uniform gravitational acceleration  $g$ . Consider topography that is initially two-dimensional and harmonic,

$$f(x) = F \cos kx \quad (1)$$

where  $x$  is the horizontal coordinate and  $k$  is the horizontal wave number. Then at  $t > 0$ , the topography  $h(x, t)$  is given by [e.g., Cathles, 1975]

$$h(x, t) = F e^{-t/\tau_0} \cos kx \quad (2)$$

where

$$\tau_0(k) = 2\eta k / \rho g \quad (3)$$

The relaxation is faster (i.e.,  $\tau_0$  is less) for lower viscosity, for smaller  $k$  or greater wavelength ( $2\pi/k$ ), and for greater gravitational acceleration.

The solution for circularly symmetric topography is analogous to (2). If the initial topographic profile is  $f(r)$ , where  $r$  is the radial coordinate, then at  $t > 0$  the topography  $h(r, t)$  is given by [Cathles, 1975]

$$h(r, t) = \int_0^\infty F(k) e^{-t/\tau_0(k)} J_0(kr) k dk \quad (4)$$

where  $J_0$  is the Bessel function of order zero,  $\tau_0(k)$  is given by (3), and  $F(k)$  is the Hankel transform of  $f(r)$ :

$$F(k) = \int_0^\infty f(r) J_0(kr) r dr \quad (5)$$

Equations (3)–(5) have been used to evaluate the effect of viscous relaxation on lunar craters by Daneš [1965], Scott [1967], and Hall *et al.* [1981] and to estimate the lifetimes of crater and basin relief on Mercury by Schaber *et al.* [1977].

In practice, the initial topographic profile in Figure 1b is represented by a discrete series at a radial distance spacing of 20 km. The Hankel transform in (5) is evaluated by quadrature using the trapezoid rule and polynomial approximations to  $J_0$  given by Abramowitz and Stegun [1964]. The integral in (4) is replaced by an equivalent sum over 200 wave numbers spaced evenly in  $k$  between wavelengths of 4000 and 40 km. The neglect of the spherical geometry of the lunar surface is likely to introduce some error in the relaxation times for the longest wavelengths (several hundred kilometers and greater) in the basin topographic spectrum.

The predicted viscous relaxation of Orientale basin topography with the half-space model for viscosity in the moon is shown in Figure 2. Profiles are given at a number of times  $t$  for the assumed values  $\rho = 2.9$  g/cm<sup>3</sup>,  $g = 162$  cm/s<sup>2</sup>, and  $\eta = 10^{25}$  P. For the profiles shown, the indicated times would increase or decrease in direct proportion to changes in the assumed value for viscosity. Note that because long-wavelength features decay faster than short-wavelength features according to (3), the overall relief of the basin and the depth of the central depression decrease faster than the local relief of individual ring structures.

A uniform half space is not, for many reasons, an adequate model of the rheology of the moon. Laboratory experiments on the creep behavior of rocks and minerals appropriate to planetary crusts and mantles indicate that the effective viscosity of such materials is strongly dependent, in general, on temperature, strain rate (or deviatoric stress), and composition [e.g., Tullis, 1979]. Figure 3 displays, as examples, the effective viscosity of olivine [Goetze, 1978] and pyroxene [Avé Lallemant, 1978] at dry conditions as functions of temperature and stress difference. While a nonlinear relationship between stress difference and strain rate has been demonstrated for creep in rock-forming minerals at stress differences of hundreds of bars to kilobars and is characteristic of flow mechanisms controlled by the movement of dislocations [e.g., Goetze, 1978], Figure 3 indicates that the variations in the effective viscosity within planets is primarily a function of temperature and only secondarily a function of the stress difference. Thus to retain the simplicity and clarity of analytical models for planetary rheology, we maintain the assumption of a Newtonian viscosity (i.e., strain rate is linearly proportional to stress difference), but we permit viscosity to vary with depth in recognition of a strong dependence of rheology on temperature.

##### Layer Over Inviscid Half Space

The next simplest model that we consider for lunar rheology is that of a layer of uniform Newtonian viscosity  $\eta$  and thickness  $H$  overlying a half space of viscosity sufficiently low so that we may regard the material as inviscid ( $\eta = 0$ ) at geological time scales. The conceptual motivation for such a model is that of a lithosphere in which viscous

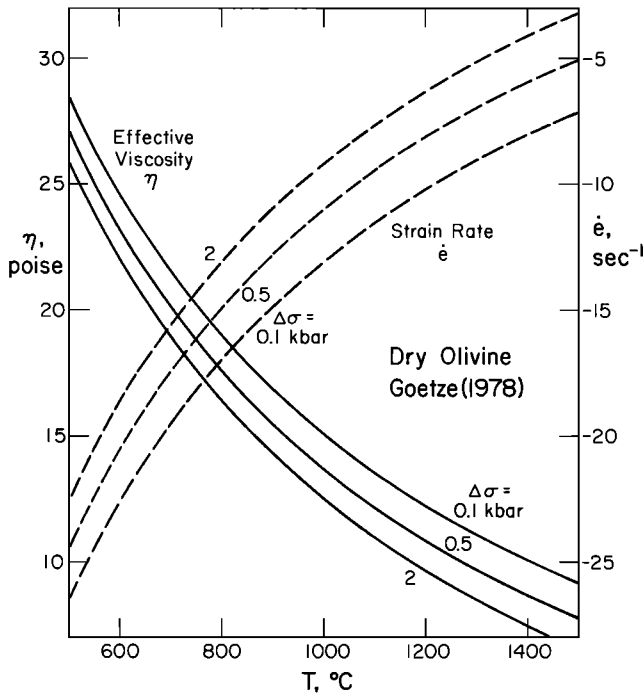


Fig. 3a

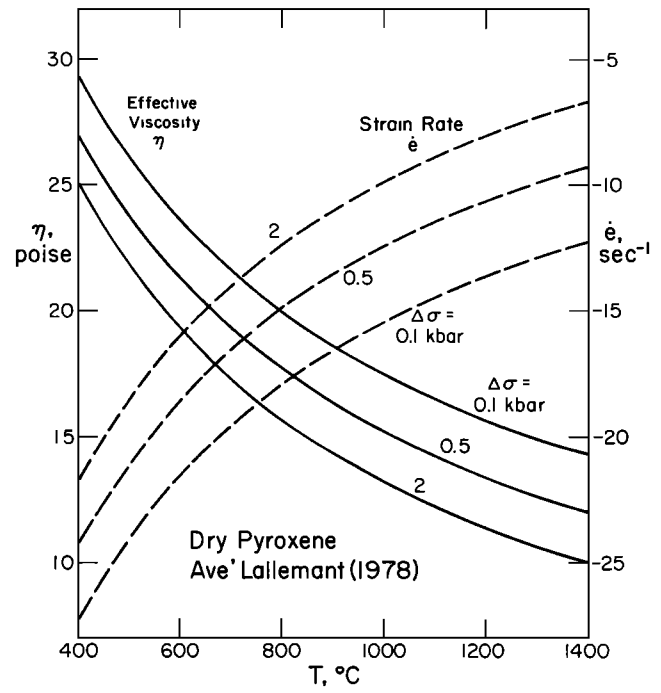


Fig. 3b

Fig. 3. Effective viscosity  $\eta$  and strain rate  $\dot{\epsilon}$  (both  $\log_{10}$ ) versus temperature  $T$  and stress difference  $\Delta\sigma$  for polycrystalline olivine (Figure 3a) and polycrystalline pyroxene (Figure 3b) at low pressures and at 'dry' conditions. The curves for olivine are from the flow law for dislocation creep given in equation (7) of Goetze [1978] and are appropriate to olivine of approximate composition  $(\text{Mg}_{0.9}\text{Fe}_{0.1})_2\text{SiO}_4$  at stress differences of 2 kbar and less and at confining pressures of 15 kbar and less. The possible effect of Coble creep [Goetze, 1978] at stress differences greater than a few hundred bars has not been considered in constructing these curves. The curves for pyroxene are based on the flow law parameters obtained by Avé Lallemand [1978] from creep measurements on 'dry' websterite (68% diopside, 32% bronzite) at stress differences less than 7 kbar and at confining pressures of 10 kbar.

processes can be important but occur on long time scales (e.g., millions of years), in contrast to the underlying asthenosphere in which, by analogy to the earth, viscous processes have much shorter characteristic times ( $10^3$  to  $10^4$  years). We ignore, for this model, any possible density contrast between the layer and the underlying half space and therefore any isostatic compensation of topography. In general, both  $\eta$  and  $H$  are free parameters. A somewhat similar model, also without isostatic compensation, was treated by Parmentier and Head [1981].

The viscous relaxation of axisymmetric topography with this model (see the appendix) is again given by equations (4) and (5) except that  $\tau(k)$  is given by

$$\tau(k) = \frac{2\eta k}{\rho g} \left[ \frac{e^{2kH} + e^{-2kH} - 4(kH)^2 - 2}{e^{2kH} - e^{-2kH} + 4kH} \right] \quad (6)$$

Thus the relaxation time differs from the half-space solution  $\tau_0(k)$ , given in (3), by the factor in brackets; that factor is plotted as a function of  $2kH$  in Figure 4. From the figure it may be seen that  $\tau(k)$  is indistinguishable from the half-space solution for  $2kH \geq 10$ ; i.e., for wavelengths  $2\pi/k$  less than the layer thickness  $H$ . For  $2kH < 10$ , viscous relaxation is faster than for the half-space solution because motion of the underlying inviscid fluid is an important component of the response. For  $2kH \ll 1$ , the factor in brackets in (6) behaves as  $(kH)^3/6$ , so that the longest wavelength topography decays at a rate substantially faster than for the half-space model. The viscosity of a planetary asthenosphere is not negligible, of course, at sufficiently short time scales ( $10^4$  years and

less). For a rheological model with a layer of viscosity  $\eta$  and thickness  $H$  overlying a half space of viscosity  $\eta_m \ll \eta$ , the time constant  $\tau(k)$  is well approximated by (3) for wavelengths less than  $H$  and approaches  $2\eta_m k/\rho g$  in the long-wavelength limit.

The viscous relaxation of Orientale topography is shown for the model of a viscous layer over an inviscid half space in Figures 5 and 6 for two values of  $H$ , 50 and 100 km, respectively. These two values are similar to the effective thicknesses of the elastic lithosphere of the moon derived from the tectonic response to mare basalt loading of mascon mare basins in the approximate time period 3.6 to 3.8 b.y. ago [Solomon and Head, 1980], times probably more recent than those over which viscous effects were important in the lunar lithosphere at spatial scales corresponding to impact basin dimensions. It is clear from Figures 5 and 6 that relaxation of long-wavelength topographic relief is considerably faster for the layer model than for the half-space model (Figure 2) and is faster for the 50-km-thick layer than for the 100-km thick layer for wavelengths of 50 km and greater.

As discussed at length in the appendix, several approximations are necessary in the derivation of (4), (5), and (6) for this model. From equations (A15) and (A22), for a harmonic load,

$$\begin{aligned} k|F| &\ll 1 && \text{for all } k \\ k|F| &\ll (kH)^3/3 && \text{for } (kH) \ll 1 \end{aligned} \quad (7)$$

For our problem of circularly symmetric loads in which the integral in (4) is replaced by a discrete sum over a finite

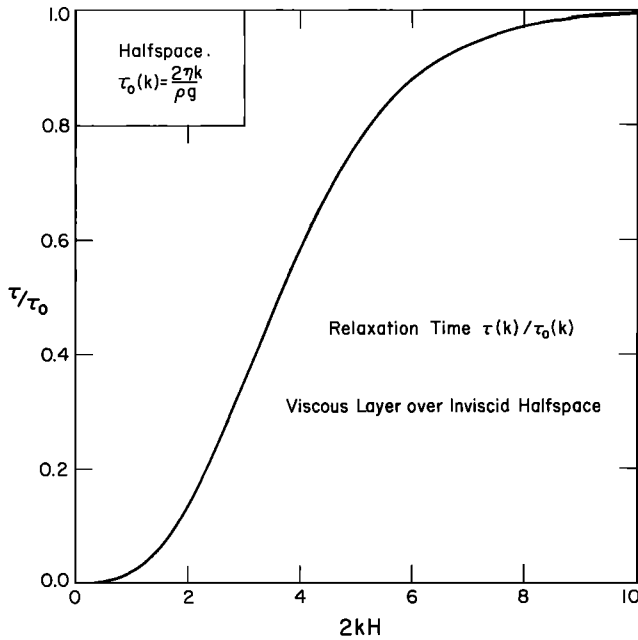


Fig. 4. Relaxation time  $\tau$  versus wave number  $k$  for a viscous layer of thickness  $H$  over an inviscid half space. The relaxation time has been normalized by the relaxation time  $\tau_0$  for a uniform half space.

number of wave numbers, the quantity  $|F(k)|$  in (7) is replaced by the coefficient of  $J_0(kr)$  in the summation. For the Orientale profile in Figure 1b, the first inequality in (7) is easily satisfied for all  $k$  and all time  $t$ ; i.e., topographic slopes are gentle. The second inequality is satisfied for all time  $t$  and for small  $k$  when  $H = 100$  km; for  $H = 50$  km and wavelengths  $2\pi/k \geq 700$  km, however, the expressions on the two sides of the second inequality in (7) are comparable in magnitude at  $t = 0$ . For these long wavelengths also, as noted above, the neglect of the spherical geometry of the lunar lithosphere introduces further errors in the relaxation problem. The longest wavelength components of the relaxation displayed for these models, particularly in Figure 5, may require some modification once these additional aspects of the problem are incorporated in the analysis.

While the model of a viscous layer over a half space of much lower viscosity provides a simplified representation of a decreasing viscosity with temperature and therefore with depth, this model and the earlier half-space model ignore any isostatic compensation of the initial basin topography. Gravity anomalies over young basins indicate that the crustal thickness beneath basins is substantially less than beneath surrounding terrain [Bowin et al., 1975; Sjogren and Smith, 1976; Thurber and Solomon, 1978]. Crustal thinning is presumably accomplished during basin formation by the combined effects of transient cavity excavation and mantle upwelling during inward collapse of the cavity and development of the outer ring scarp [Head, 1977; Melosh and McKinnon, 1978; Phillips and Dvorak, 1981]. Mantle uplift beneath the basin interior provides partial to complete compensation of the mass deficiency of the basin depression [Bowin et al., 1975; Sjogren and Smith, 1976; Phillips and Dvorak, 1981]; this compensation can affect the viscous relaxation process substantially and should be included in any discussion of relaxation of impact basin topography.

Layer With Isostatic Compensation

The final analytical model we consider for lunar rheology is that of a layer of uniform viscosity  $\eta$ , density  $\rho$ , and thickness  $H$  overlying an inviscid half space of greater density  $\rho_m = \rho + \Delta\rho$ . For this model, the topographies at the surface and at the depth of the density contrast are coupled through the equations of motion and the boundary conditions; see the appendix. The topography at  $t = 0$  at the mean depth  $H$  must be given as an initial condition; we assume a specified fraction  $c$  ( $0 \leq c \leq 1$ ) of local Airy isostatic compensation in order to relate the initial depth of the density contrast to the initial surface topography. We are restricted with this model to have the depth of isostatic compensation coincide with the base of the high viscosity layer, but with this restriction we can obtain an analytical solution that permits a full exploration of the effects of both a decrease in viscosity with depth and initial isostatic compensation of topography on the viscous relaxation problem.

The solution for topography  $h(r, t)$  at  $t > 0$  is given, following the appendix, by

$$h(r, t) = \int_0^\infty [F_1(k)e^{-t/\tau_1(k)} + F_2(k)e^{-t/\tau_2(k)}] J_0(kr) k dk \quad (8)$$

In this relation  $F_1(k)$  and  $F_2(k)$  are given by equations (A27), (A2), (A24), and (A26), and satisfy

$$F_1(k) + F_2(k) = F(k) \quad (9)$$

where  $F(k)$  by (5) is the Hankel transform of the initial topographic profile  $f(r)$ . The relaxation of a viscous layer overlying a half space of different density and viscosity has been treated in somewhat different form by Ramberg [1968] and by Dvorak and Phillips [1975]; the relaxation with time of a large lunar crater according to the Dvorak-Phillips treatment was displayed by Phillips and Lambeck [1980].

Two distinct time constants in (8),  $\tau_1(k)$  and  $\tau_2(k)$ , govern the relaxation of topographic relief [cf. Ramberg, 1968]. The time constants are each proportional to  $\eta/g$  and are distinct functions of  $\rho$ ,  $\Delta\rho$ ,  $H$ , and  $k$ ; see equations (A26) and (A24). The two time constants are plotted as functions of  $k$  in Figure 7 for the case  $\rho = 2.9$  g/cm<sup>3</sup> and  $H = 50$  km [Toksöz et al.,

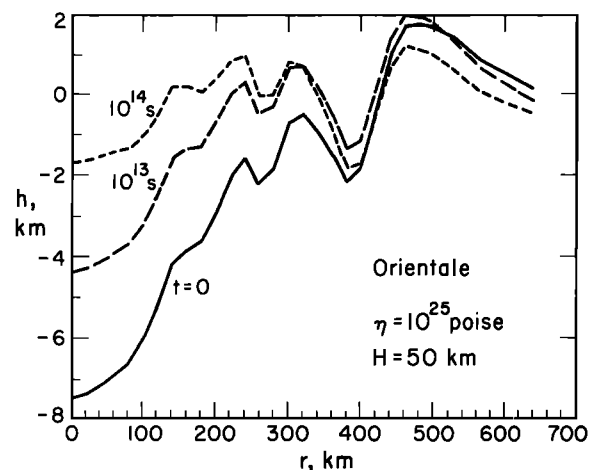


Fig. 5. Viscous relaxation of Orientale basin topography for a 50-km-thick layer of viscosity  $\eta = 10^{25}$  P over an inviscid half space. Profiles are shown at  $t = 0$ ,  $10^{13}$  s (0.3 m.y.) and  $10^{14}$  s (3 m.y.); these times scale linearly with the assumed layer viscosity.

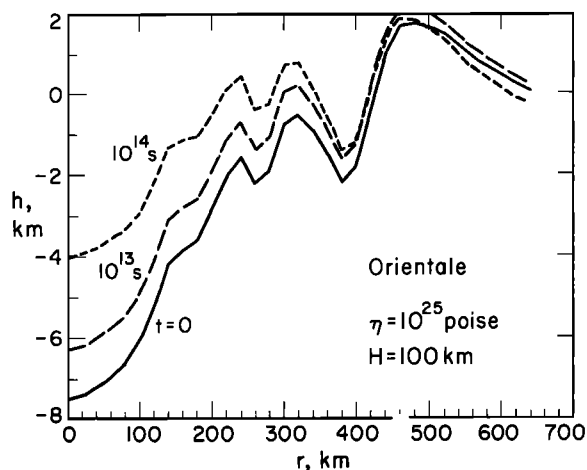


Fig. 6. Viscous relaxation of Orienteale basin topography for a 100-km-thick layer of viscosity  $\eta = 10^{25}$  P over an inviscid half space. Profile times and their scaling with  $\eta$  are as in Figure 5.

1974; Koyama and Nakamura, 1979]. The time constant  $\tau_2$  behaves similarly to the time constant (equation (6)) for the case of the viscous layer overlying an inviscid half space of the same density:  $\tau_2 \sim k^4$  for small  $k$  and is equal to the time constant  $\tau_0 \sim k$  for the half-space case at large  $k$ . The time constant  $\tau_1$ , however, is considerably larger than  $\tau_0$  at all wave numbers, particularly at small  $k$ . As  $k \rightarrow 0$ ,  $\tau_1$  approaches a constant (equation (A33)), a function of  $\rho$ ,  $\Delta\rho$  and  $H$  but not of  $k$ . At large  $k$ ,  $\tau_1$  is proportional to  $k$  and exceeds the half-space time constant by the factor  $\rho/\Delta\rho$ .

Thus partial to complete isostatic compensation of initial basin topography results in a considerable deceleration of viscous relaxation of relief, compared to models without isostatic effects, for a fraction of the initial relief that depends on the degree of compensation. As shown in equation (A35), the fraction  $F_1$  of  $F$  that decays with the time constant  $\tau_1$  approaches unity in the long-wavelength limit for complete initial compensation ( $c = 1$ ). Further, for any value of  $c$ , the topographic relief decaying with time constant  $\tau_1$  is always completely compensated for small  $k$ ; i.e., the long-wavelength basin topography is isostatic for  $t \gg \tau_2$  no matter what the initial degree of compensation.

These conclusions are illustrated in Figures 8 and 9. The case with complete initial compensation ( $c = 1$ ) is shown in Figure 8. Relaxation of relief is much slower than in Figures 2, 5, or 6, with substantial long-wavelength relief (4 km) remaining after 3 b.y. ( $10^{17}$  s) for a layer viscosity of  $10^{25}$  P. Note that in comparison to Figures 2 or 5, the topography in the relaxed profiles is 'smoother.' This is because of the comparatively weak dependence of  $\tau_1$  on  $k$  (see Figure 7) over the wave numbers of interest; i.e., the rate of relaxation at long wavelengths is greater, compared to the short wavelengths, than for the simple half-space model or for the model with no density contrast at the base of the viscous layer.

The case with initial topography only half compensated by Airy isostasy ( $c = 0.5$ ) is shown in Figure 9. There is a rapid partial relaxation of initial relief (governed by time constant  $\tau_2$ ), followed by a much slower relaxation of the remainder. The total relief at 3 b.y. (for  $\eta = 10^{25}$  P) is about 2 km, or half that in Figure 8 at the same time. The case with initially

uncompensated topography, but with a density contrast at the base of the layer, behaves similarly to that in Figure 5 except for a small fraction ( $\Delta\rho/\rho_m$ ) of the long-wavelength topographic relief that relaxes at the longer time constant  $\tau_1$ .

The assumptions necessary to derive (8) and (9) and the models shown in Figures 8 and 9 include, from equations (A15) and (A22) and by analogy to relations (7),

$$\begin{aligned} k|F| &\ll 1 \\ k|G| &\ll 1 \end{aligned} \tag{10}$$

$$\left| kF + \frac{\Delta\rho}{\rho} kG \right| \ll (kH)^3/3$$

where  $G(k)$  is the Hankel transform of the profile of topographic relief at the base of the layer (see the appendix). Strictly,  $F$  and  $G$  are the coefficients of  $J_0(kr)$  in the summation representation of (8) and in the analogous expression for relief at the bottom of the viscous layer. The first two inequalities hold for the Orienteale profile for all  $k$  and all  $t$ . The third inequality in (10) holds for a greater range of cases than does the analogous inequality in (7) because  $G$

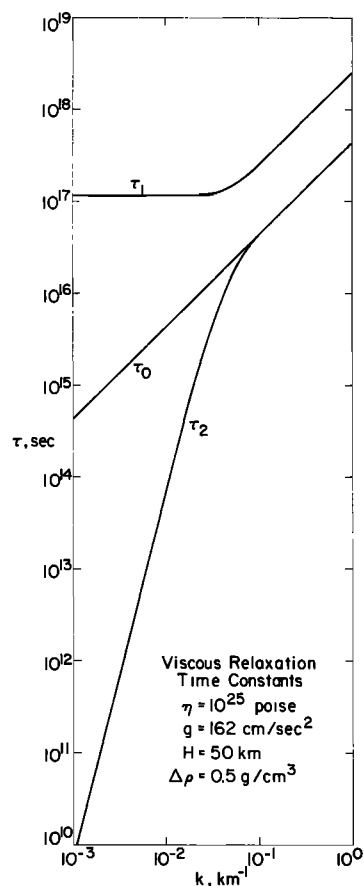


Fig. 7. Time constants  $\tau_1$  and  $\tau_2$  versus horizontal wave number  $k$  for the problem of relaxation of topography on a viscous layer overlying an inviscid half space of greater density, both in a uniform gravitational field. The layer has viscosity  $\eta = 10^{25}$  P, density  $\rho = 2.9$  g/cm<sup>3</sup>, and thickness  $H = 50$  km; the half space has density  $\rho + \Delta\rho = 3.4$  g/cm<sup>3</sup>; the gravitational acceleration is 162 cm/s<sup>2</sup>. Also shown is the time constant  $\tau_0(k)$  for the case of a half space of uniform viscosity  $\eta$  and density  $\rho$ . All time constants are proportional to  $\eta$  and inversely proportional to  $g$ ; the long-wavelength limit of  $\tau_1$  is inversely proportional to  $H$ .



Fig. 8. Viscous relaxation of Orientale basin topography for a viscous layer over an inviscid half space and for complete Airy isostatic compensation of topography as an initial condition. The layer has viscosity  $\eta = 10^{25}$  P, density  $\rho = 2.9$  g/cm<sup>3</sup>, and thickness  $H = 50$  km; the half space has density  $\rho + \Delta\rho = 3.4$  g/cm<sup>3</sup>. Profiles are shown at  $t = 0$ ,  $10^{16}$  s (300 m.y.),  $3 \times 10^{16}$  s (1 b.y.), and  $10^{17}$  s (3 b.y.); these times scale linearly with the assumed layer viscosity.

and  $F$  are of opposite sign in the presence of partial to complete isostatic compensation. In particular, the left-hand side of the third inequality is identically zero at all times for  $c = 1$  and at  $t \gg \tau_2$  for any  $c$ .

A major question for the application of this viscous relaxation model to ancient lunar basins is the value of  $c$ , i.e., the degree of isostatic compensation of lunar basins prior to mare basalt fill. There are, unfortunately, only limited gravity and topographic data available to answer this question. Further, the estimation of the initial degree of compensation is sensitive to the depths of all mass excesses and deficiencies beneath present basins, quantities poorly resolved by gravity field measurements at spacecraft altitudes. For the Orientale basin, *Sjogren and Smith* [1976] considered a number of simple models that matched existing gravity data with varying degrees of success. For a model in which mass anomalies are at the lunar surface, the central basin region of Orientale (within 150 km radial distance) contributes  $3 \times 10^{20}$  g excess mass, the region between 150 and 350 km radial distance contributes a mass deficiency of  $-17 \times 10^{20}$  g, and the outer ring (350–620 km radial distance) contributes an excess mass of  $7 \times 10^{20}$  g [*Sjogren and Smith*, 1976, Table 1]; there is a net mass deficiency of  $-7 \times 10^{20}$  g. This result may be compared to the mass deficiency calculated from the topography. If we assume that Figure 1b represents circularly symmetric topography of density 2.9 g/cm<sup>3</sup>, then there is a total mass deficiency of  $-19 \times 10^{20}$  g; the region  $r = 0$  to 430 km contributes  $-38 \times 10^{20}$  g, while the outer ring structure between  $r = 430$  and 640 km contributes an excess  $19 \times 10^{20}$  g. Thus in the surface mass model for Orientale gravity, the mass deficiency is presently 38% of the topographic mass deficiency and would have been as high as 50% prior to mare basalt fill.

*Sjogren and Smith* [1976] obtained an improved fit to the gravity data for models including a large fraction of the excess mass at the base of the lunar crust; i.e., including a thinned crust beneath the basin to provide partial compensation of the topographic depression. For these models the net

mass excluding mare fill is either negative ( $-8 \times 10^{20}$  g for their model 5) or small ( $0.2 \times 10^{20}$  g for their model 2). Even though the compensation of Orientale basin topography is not local, we may conclude from these results that the net prefill mass deficiency for Orientale was considerably smaller than the mass deficiency of the present topography because of partial compensation by crustal thickness variations.

In all, the cases  $c = 0.5$  and  $c = 1$  appear to bracket the most likely Airy isostatic model for the Orientale basin and therefore for unmodified lunar basins in general. Gravity analyses for other lunar basins support this conclusion. The preferred model of *Bowin et al.* [1975] for the Serenitatis basin is in isostatic equilibrium prior to mare fill. *Phillips and Dvorak* [1981] give models for the Grimaldi basin in which the pre-mare topographic depression is 62 to 100% compensated. Thus the available gravity data over lunar basins indicate that early basin topography was at least partially compensated; this compensation must be included in the calculation of subsequent viscous relaxation of topographic relief.

#### APPLICATION TO ANCIENT LUNAR BASINS

We now apply the model of viscous relaxation to the topography of ancient (i.e., pre-Nectarian) lunar basins. Specifically, we assume that the topographic profiles of ancient basins shortly after their formation were similar to the present profile of Orientale, and we test the hypothesis that the ancient basin topography was subsequently modified by viscous relaxation during the time interval (between basin formation and perhaps 3.8 b.y. ago) when near-surface temperatures were high and the effective viscosity of the lunar lithosphere was low enough for creep to be important at geological time scales.

*Tranquillitatis basin.* We first consider the Tranquillitatis basin (Figure 10), one of the oldest identifiable basins on the lunar nearside [*Stuart-Alexander and Howard*, 1970; *Hartmann and Wood*, 1971; *Wilhelms*, 1981]. *Stuart-Alexander and Howard* [1970] have suggested that the irregular Mare Tranquillitatis fills two old basins, with the western basin the younger of the two. *Wilhelms and McCauley*

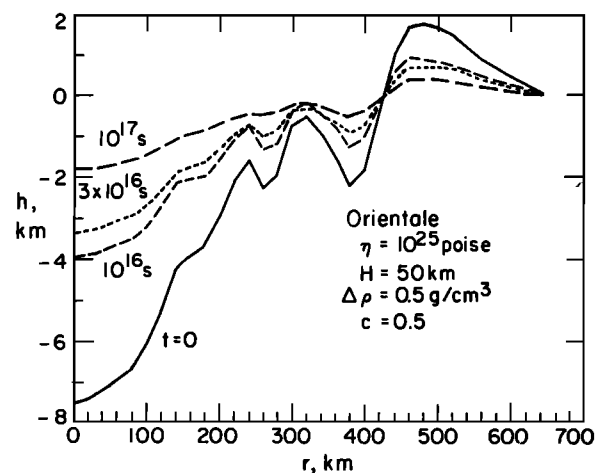


Fig. 9. Viscous relaxation of Orientale basin topography for a viscous layer over an inviscid half space and for 50% ( $c = 0.5$ ) isostatic compensation of topography as an initial condition. Other physical parameters and profile times and their scaling with layer viscosity  $\eta$  are as in Figure 8.

[1971], in contrast, show only one ancient Tranquillitatis basin, marked by a major ring structure of about 340 km radius centered approximately at 7.5°N, 29°E, and a remnant of an outer ring of about 460 km radius in the northeast quadrant. There is also a prominent system of linear and arcuate rilles peripheral to the western half of the mare [Scott *et al.*, 1975]; many of these rilles are concentric to a similar point (8°N, 29°E). In younger lunar mascon basins, such rilles are concentric with the inner depression and the rings forming the major basin topography [Solomon and Head, 1980]. We therefore follow the basin identification of Wilhelms and McCauley [1971]. On the basis of present topography we identify the ring of major massifs at  $r \approx 340$  km with the outer Rook Mountains of Orientale and the outer ring trace at  $r \approx 460$  km with the Cordillera Mountains. By this assignment the ancient Tranquillitatis basin has very nearly the same horizontal dimensions as Orientale.

The present topography of the Tranquillitatis basin region is known to an accuracy of a few hundred meters or better from Apollo photogrammetric measurements. A representative profile is shown in Figure 10b. The elevations are taken from the 1:1,000,000 scale Lunar Map 60 [Schirmerman, 1973]. Dvorak and Phillips [1979] also show an earth-based radar topographic map for a portion of the Tranquillitatis basin; the radar data have not been used because they are referenced to a floating datum and contain the effects of an uncertain regional slope (S. H. Zisk, personal communication, 1981).

Several processes have acted to modify this topography since basin formation in addition to viscous relaxation. The basin has been modified by the emplacement of ejecta from younger basins in the immediate vicinity, including Nectaris, Crisium, Serenitatis, and Imbrium, among others. The profile in Figure 10b is in a radial direction that should have been least affected by younger basin deposits; on the basis of estimates for ejecta thickness versus range, the total thickness in this portion of Tranquillitatis of ejecta from other basins is not likely to exceed several hundred meters [McGetchin *et al.*, 1973]. Pre-mare volcanism may also have modified this region [Morris and Wilhelms, 1967], but its presence and significance cannot readily be established.

The Tranquillitatis basin has been partially filled by basalt to produce Mare Tranquillitatis. The thickness of mare basalt in the Tranquillitatis region has been estimated and mapped by DeHon [1974] from the rim heights of partially flooded craters. While it is difficult to demonstrate that such craters were produced on the pre-mare basin surface, these estimates of basalt thickness are similar to those derived from gravity data and the assumption of complete isostatic compensation of pre-mare topography [Thurber and Solomon, 1978], so we accept the basalt thickness maps of DeHon [1974] for the purposes of estimating pre-mare topography. The profile in Figure 10b shown as a dashed line corresponds to the topography at the base of the mare fill according to these estimates. The topography is complicated in the Lamont region, which may be part of a structural trough in the western part of the basin and may locally have subsided by at least 1.5 km in response to a small mascon [Dvorak and Phillips, 1979]. Except for the Lamont area, the topography at the base of the mare fill shown in Figure 10b represents our best estimate of a representative topographic profile for an ancient lunar nearside basin of dimensions originally similar to those of Orientale.

In Figure 11 we show a comparison of the topographic profile of Tranquillitatis with a profile calculated from the viscous relaxation of Orientale topography, using the model depicted in Figure 8 (complete initial isostatic compensation). The calculated profile is shown for a value of  $t/\eta$  ( $1.5 \times 10^{-8}$  s/P) that matches the depth to the base of the mare at the center of the ancient basin; this model profile underestimates by as much as 2 km the depth to the base of the mare basalt within the region of subsidence in the vicinity of Lamont. A somewhat smaller value of  $t/\eta$  would be obtained if we attempted to provide a best fit to the Tranquillitatis profile at the base of the mare basalt without regard to the post-mare subsidence of the Lamont region.

We conclude that the topographic profile of the Tranquillitatis basin is consistent with substantial viscous relaxation of relief between the time of basin formation and the emplacement time of the oldest surface mare basalt units. Because the long-wavelength topography remains in isostatic equilibrium during relaxation, a prediction of the relaxation model is that the crustal thickness beneath Tranquillitatis should be significantly greater than beneath the central portions of the youngest basins. An appropriate difference in crustal thickness, in fact, is present on the basis of an inversion of gravity and topographic data for the lunar nearside [Thurber and Solomon, 1978].

The quantity  $t/\eta$  should be regarded as follows. Because the effective viscosity of the lunar crust almost certainly increased, perhaps rapidly, with time following the period of high near-surface temperatures associated with impact heating and mare volcanism, substantial viscous relaxation was restricted in time to that period when the viscosity was sufficiently low for viscous creep to have been geologically important in the upper crust. Thus  $\eta$  is approximately the effective viscosity of the crust during the time of highest near-surface temperatures, and  $t$  is the time interval over which the viscosity was near to this value. The preserved large relief of Orientale (Figure 1), the lack of isostatic compensation of the Apennine mountains forming part of a ring structure of the Imbrium basin [Ferrari *et al.*, 1978], and the support by finite strength of the mascon loads in young nearside impact basins [Solomon and Head, 1980] indicate that the time interval over which viscous relaxation was important for nearside basins was probably at most a few hundred million years. For Tranquillitatis, in particular, important viscous relaxation of topography was completed prior to emplacement of Apollo 11 basalts, 3.7 to 3.8 b.y. in age [e.g., Wasserburg *et al.*, 1977], which appear to be typical of the oldest mare basalt deposits preserved at the surface of Mare Tranquillitatis [Boyce, 1976].

The derived value for  $t/\eta$  is within the range of values estimated for this quantity ( $0.4$  to  $5.1 \times 10^{-8}$  s/P) from the topographic profiles for lunar floor-fractured craters of diameter 16 to 40 km [Hall *et al.*, 1981]. This agreement is somewhat surprising because these craters are younger than the Tranquillitatis basin and the viscous relaxation of their topography is sensitive primarily to the viscosity only in the upper third to half of the lunar crust. On both of these grounds, the value of  $\eta$  controlling viscous relaxation of these floor-fractured craters might be expected to be larger than the effective crustal viscosity governing relaxation of a larger and older impact basin. The agreement may, however, be only coincidental. Many of the craters considered by Hall *et al.* [1981] are in regions distant from Tranquillitatis,

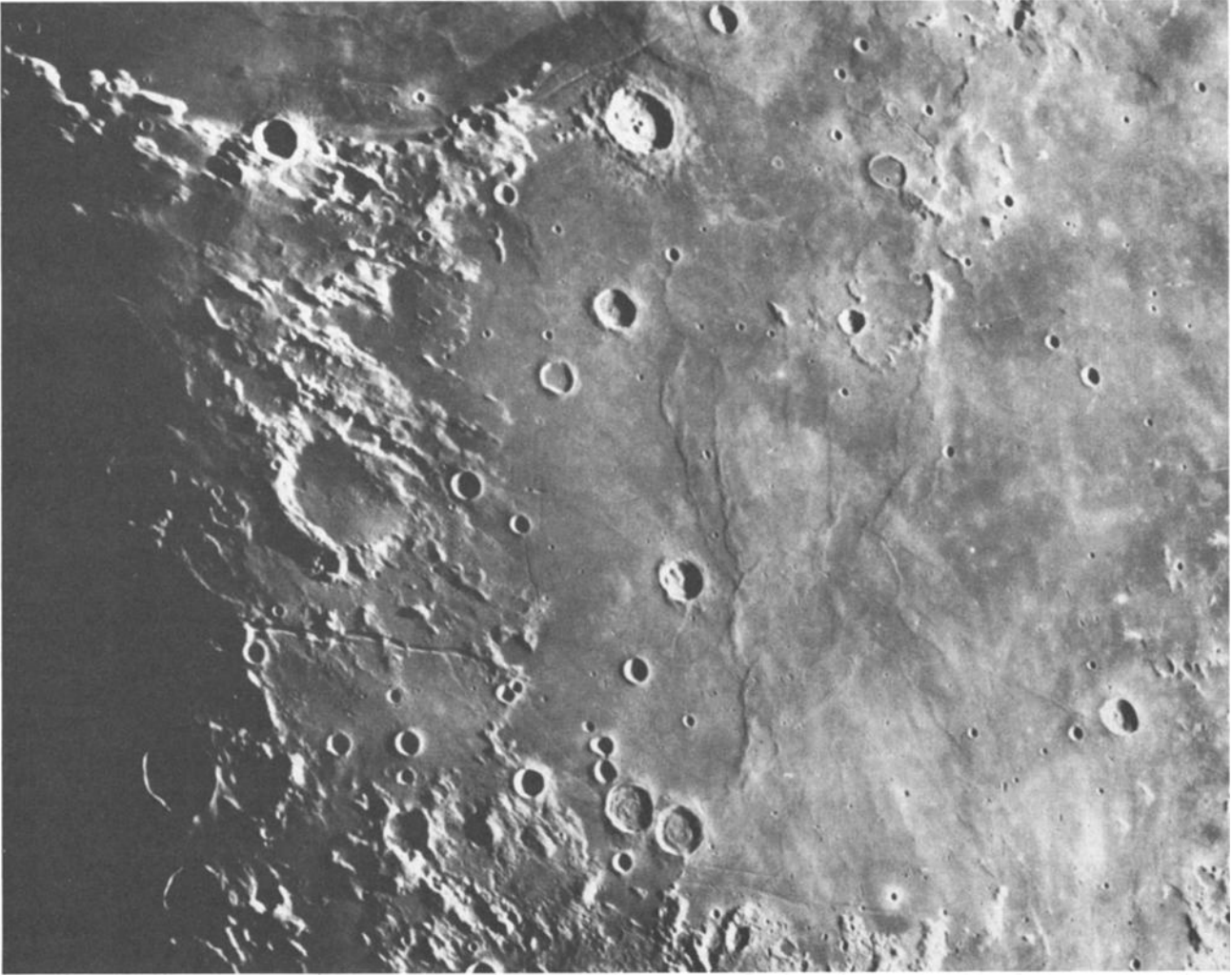


Fig. 10a. The lunar Tranquillitatis basin. Earth-based photograph; plate C2571D8 from *Kuiper et al.* [1967].

although two (Ritter and Sabine) are located at the edge of the Tranquillitatis mare deposits. It is also worth recalling that only the quotient  $t/\eta$  can be estimated for the viscous relaxation process; neither  $\eta$  nor the time interval  $t$  of important relaxation can be estimated separately. Probably the explanation for the apparently similar values of  $t/\eta$  for an ancient large basin and for younger, smaller craters lies in the observation [Schultz, 1976; Hall et al., 1981] that the extent of modification of contemporaneous and neighboring craters on the moon can be quite variable. The high near-surface temperatures leading to topographic modification of many floor-fractured craters apparently were localized to regions and scales smaller than the dimensions of large impact basins. By this reasoning, the relaxation of a basin would be governed by a weighted average of the heterogeneous viscosity of the underlying crust, an average that may be considerably larger than the viscosity of local regions of higher than average temperature associated with volcanism, igneous intrusions, or impact heating. Note that the derived value of  $t/\eta$  for Tranquillitatis would not have been obtained had we applied a model for viscous relaxation of basin topography that neglected the effect of initial isostatic compensation; for such a model the best fitting value for  $t/\eta$  would have been smaller by 3 to 4 orders of magnitude.

The extent of modification of topographic relief in the Tranquillitatis basin appears to be representative of other pre-Nectarian basins on the lunar nearside. The Fecunditatis basin, for instance, of similar size, age, and state of preservation as Tranquillitatis [Wilhelms, 1981], has similar topographic relief both on the present surface and on the basin surface with mare basalt removed [DeHon and Waskom, 1976]. The largest and oldest proposed nearside basin of pre-Nectarian age is the 'Gargantuan' or Procellarum basin [Cadogan, 1974; Whitaker, 1981; Wilhelms, 1981], which has a postulated outer ring of diameter 3200 km [Whitaker, 1981]. Though the area encompassed by this ancient ring saw the subsequent formation of several major basins (Tranquillitatis, Serenitatis, Imbrium), the barely discernible present topography associated with the Procellarum basin and its ring structures is consistent with the large size and age of this basin and with a mean crustal viscosity similar to that in the Tranquillitatis region for the time period during which significant relaxation occurred.

*South Pole-Aitken basin.* On the southern farside of the moon is one of the largest identified lunar basins [Howard et al., 1974], and one of the oldest [Wilhelms, 1981], named the South Pole-Aitken basin by Stuart-Alexander [1978]. The basin is outlined by isolated and subdued mountain remnants

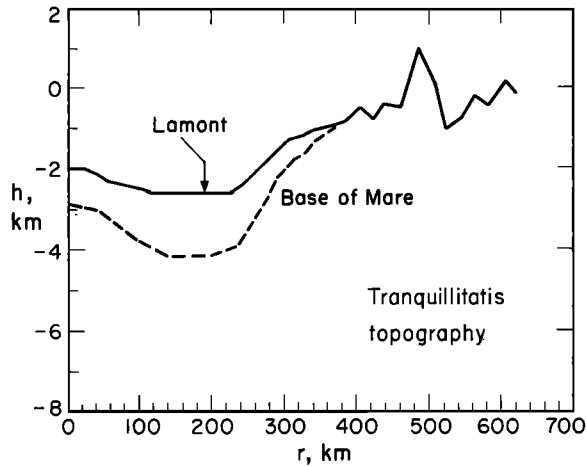


Fig. 10b. Topographic profile of the Tranquillitatis basin. The profile (solid line) extends southwest from  $8^{\circ}\text{N}$ ,  $29^{\circ}\text{E}$  ( $r = 0$ ) to  $0^{\circ}\text{N}$ ,  $10^{\circ}\text{E}$ ; topographic data are from Lunar Map 60. The datum  $h = 0$  is taken as the characteristic elevation (1738.0 km lunar radius) of nearside highlands in the vicinity of the terminus of the profile. Also shown (dashed line) is the inferred base of the mare basalt fill along the same profile, from the basalt isopach map of DeHon [1974]. The Lamont region is an area of anomalously thick mare fill, positive free air gravity, and a concentration of tectonic features, particularly mare ridges; this region has probably subsided relative to the rest of the basin [Dvorak and Phillips, 1979].

that define a ring 2000 km in diameter (Figure 12a) centered approximately at  $50^{\circ}\text{S}$ ,  $180^{\circ}\text{W}$  [Stuart-Alexander, 1978]. Limited topographic data were obtained for this basin by the laser altimetry experiment on the Apollo 15 subsatellite [Kaula et al., 1973], which made several nearly east-west traverses of the basin near latitude  $25^{\circ}\text{S}$ , considerably north of the basin center.

The laser altimetry data indicate that the South Pole-Aitken basin is a huge depression with the deepest regions as much as 8 km below the level of the surrounding farside highland terrain [Kaula et al., 1973]. A representative topographic profile, for the portion of the basin for which altimetric information is available, is shown in Figure 12b. The large dimensions and relief of this basin, in striking contrast to the Procellarum and smaller pre-Nectarian basins on the frontside of the moon, suggest that the extent of viscous relaxation has been less on the lunar farside than for nearside basins of comparable age. To quantify this result, we need to obtain an estimate of the original topographic profile of the South Pole-Aitken basin by analogy with Orientale. For this purpose we identify the 2000-km ring structure for the South Pole-Aitken basin with the Cordillera Mountain ring of Orientale, although somewhat larger estimates (2500–2600 km) for the outer ring diameter have also been proposed [Wood and Gifford, 1980; Wilhelms, 1981]. To estimate the topographic relief of South Pole-Aitken prior to any modification, we use the Orientale profile in Figure 1a with all horizontal dimensions scaled by 20/9 or 2.2 and all vertical dimensions scaled according to the depth-diameter relation of Pike [1980] for large craters; i.e. vertical dimensions scale as  $(20/9)^{0.301}$  or 1.27. Such a scaling for vertical relief is only an approximation. For instance, Pike [1980] has shown that rim height scales somewhat differently with diameter than crater depth. Further, the initial topography of backside basins may have differed from those on the

frontside because of different lithospheric or crustal thicknesses. Considering the large uncertainties inherent in extrapolating existing crater dimensions to 2000-km-diameter basins, the scaling relations adopted here should be regarded only as a reasonable working model.

The Orientale topography, so scaled to the dimensions of the South Pole-Aitken basin, is shown in Figure 13. This profile is compared to the present topography, taken from Figure 12b but plotted as a function of radial distance from the assumed basin center at  $50^{\circ}\text{S}$ ,  $180^{\circ}\text{W}$ . There is an uncertainty of at least 1 km in the zero elevation datum used to plot the present topographic profile for the South Pole-Aitken basin. Further, there are no topographic data at radial distances from basin center of less than 700 km. Nonetheless, it is clear that the scaled Orientale profile does not provide a good starting topographic model for the South Pole-Aitken basin, which has greater relief than does the scaled Orientale profile at similar radial distance ranges. At fault may be the chosen ring assignment for the South Pole-Aitken basin, or the assumption that the initial topography of this large ancient basin can be simply scaled from that of Orientale.

Also shown in Figure 13 are topographic profiles calculated under the assumptions of an initial profile as shown and a thickness  $H = 100$  km for the low-density, high-viscosity layer to account for the generally greater crustal thickness thought to occur on the lunar farside compared to the nearside [Kaula et al., 1973, 1974]. A significant amount of viscous relaxation, which would follow from  $t/\eta \geq 10^{-9}$  s/P, yields a predicted topographic profile even less like the present profile than the profile scaled from Orientale geometry with no relaxation. A significant amount of relaxation is also precluded by the present topography if the 2000-km-diameter ring of the South Pole-Aitken basin is the analog of one of the inner rings of Orientale, i.e., if the South Pole-Aitken basin was originally larger and deeper than assumed here.

Thus while viscous relaxation appears to have been an important modification process for impact basins (and large craters) on the lunar nearside, its importance was substantially less for topographic relief on the lunar farside. In

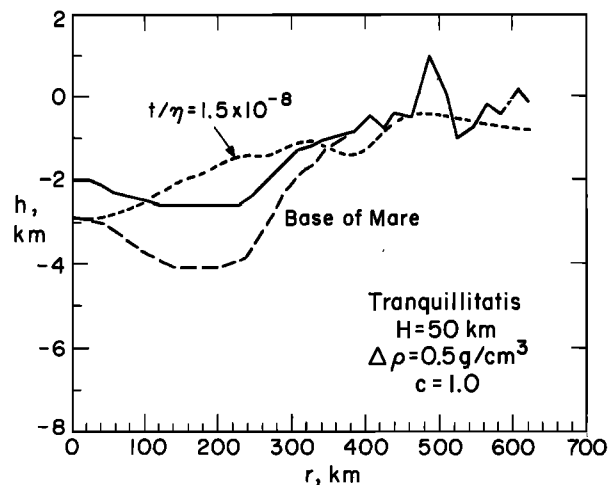


Fig. 11. Comparison of the Tranquillitatis topographic profile from Figure 10 with the profile predicted from viscous relaxation of Orientale, using the model in Figure 8. The predicted profile is shown for  $t/\eta = 1.5 \times 10^{-8}$  s/P.

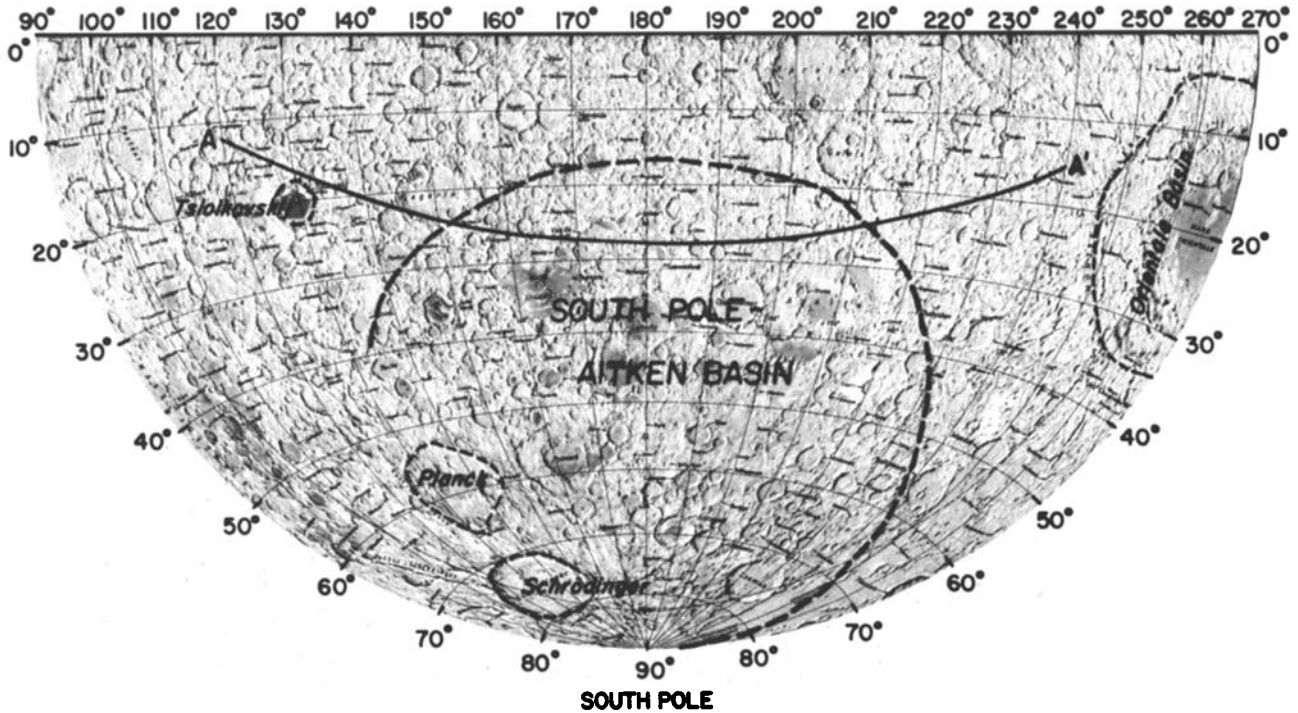


Fig. 12a. Location of the ancient South Pole-Aitken basin on the lunar farside. The ring location is after *Stuart-Alexander [1978]*. The orbital track labeled AA' is that for which laser altimetry data are shown in Figure 12b.

particular, the topographic relief preserved for the farside South Pole-Aitken basin is considerably greater than for the nearside Tranquillitatis basin, despite the greater age and size of the former feature [Wilhelms, 1981]. The most straightforward explanation of the quantitative comparison of viscous relaxation for the two basins is that crustal viscosities were at least a factor of 10 higher on the farside than on the nearside over the time interval during which viscous processes were regionally important for the lunar crust and lithosphere.

The higher crustal viscosities on the lunar farside in pre-Nectarian time were most likely a result of lower near-surface temperatures. From Figure 3, a difference in mean crustal temperatures of as little as 50°-100°C would be sufficient to account for the required nearside-farside difference in effective viscosities. There is alternatively the possibility that the great relief of the South Pole-Aitken basin may be due to incomplete collapse of the transient cavity because

of a thicker lithosphere on the farside than on the nearside [Melosh and McKinnon, 1978; Head and Solomon, 1980]; such a possibility still implies lesser average crustal temperatures on the farside at the time of formation of the oldest preserved basins. On the basis of the response of the lunar lithosphere to mascon loads in the time interval 3.6 to 3.8 b.y. ago, *Solomon and Head [1980]* estimated that the effective elastic lithosphere and thus the near-surface thermal gradient varied by at least a factor of 3 over the lunar nearside hemisphere. The results of the present work extend to the lunar farside the regions for which we now have evidence for lateral heterogeneity in lithospheric temperatures early in the history of the moon.

There are a variety of processes that may have contributed to a difference in the mean temperature of the crustal portion of the lithosphere between the nearside and farside of the moon at about 4 b.y. ago. The observed offset between the lunar centers of mass and figure indicates that the process of

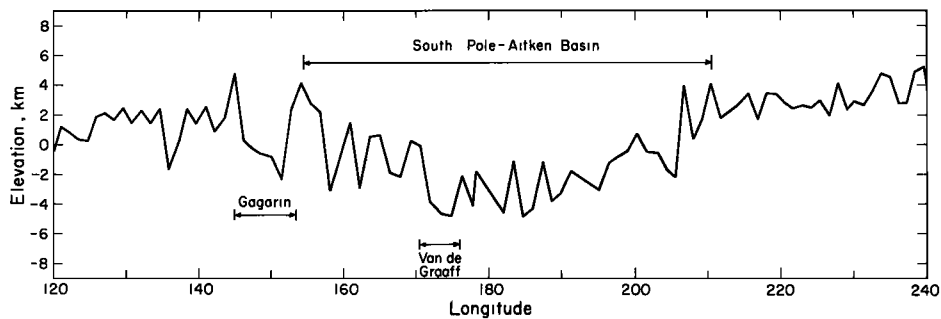


Fig. 12b. Apollo 15 laser altimeter profile (revolution 15) across the South Pole-Aitken basin and surrounding highlands [Kaula et al., 1973]. The location of the craters Gagarin and Van de Graaff are also indicated. The edge of the South Pole-Aitken basin is taken as the ring structure shown in Figure 12a.

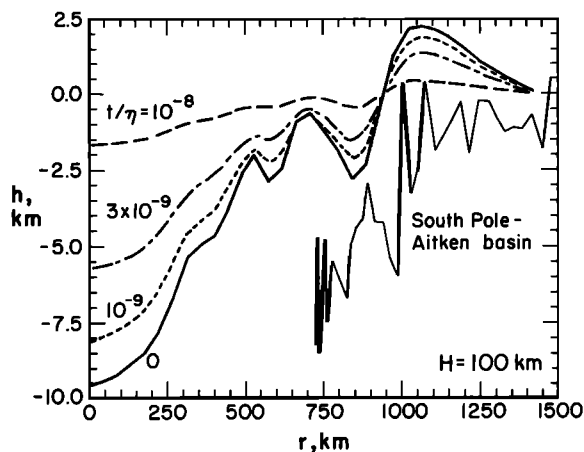


Fig. 13. Viscous relaxation of a topographic profile of Orientale scaled to the 2000-km diameter of the South Pole–Aitken basin (see text). Relaxed profiles are shown for several values (in  $s/P$ ) of  $t/\eta$ ; for  $\eta = 10^{25}$  P these correspond to  $10^{16}$  s (300 m.y.),  $3 \times 10^{16}$  s (1 b.y.), and  $10^{17}$  s (3 b.y.). A layer thickness  $H = 100$  km has been assumed. Also shown is the present topography of the South Pole–Aitken basin, taken from the laser altimetry data in Figure 12b between longitudes  $180^\circ$  and  $240^\circ$ E and plotted versus radial distance  $r$  from basin center. The datum  $h = 0$  is taken as the average elevation (lunar radius 1741.6 km) along this profile between radial distances of 1500 and 1800 km.

differentiation of the outer portions of the moon led to a nearside-farside asymmetry in crustal thickness [Kaula *et al.*, 1973, 1974], crustal density [Solomon, 1978], mantle density [Wasson and Warren, 1980], or some combination of all three [e.g., Stevenson, 1980]. This asymmetry in differentiation may also have been responsible for the greater surface concentrations of radioactive elements on the lunar nearside [Trombka *et al.*, 1977]. As a direct result either of the differentiation process itself or of the consequent distribution of radioactive elements in the near-surface regions of the moon, a nearside-farside asymmetry in crustal temperatures early in lunar history would be an expected result.

A number of additional processes may have served to maintain higher crustal temperatures and thinner lithosphere on the lunar nearside for an extended period of time. The great majority of the youngest large lunar basins, for reasons unknown, are on the nearside [Hartmann and Wood, 1971; Wilhelms, 1979], so both the impact heating associated with basin formation [O'Keefe and Ahrens, 1977] and the heating by uplift of mantle isotherms during transient cavity collapse and ring formation [Bratt *et al.*, 1981] would also have been concentrated on the nearside during this time interval. The impact event that produced the 3200-km-diameter Procellarum basin [Whitaker, 1981] may alone have contributed substantially to maintaining the hemispherical asymmetry. The vast majority of mare basalt eruptions and of floor-fractured craters, many of which are associated with mare-type volcanism, also occurred on the lunar nearside. Mare volcanism is both a manifestation of high temperatures at depth and a mechanism for heating the shallow crustal regions surrounding volcanic units, eruptive centers, and igneous intrusions. Thus some nearside-farside difference in shallow crustal temperatures may have persisted throughout the time interval between crustal formation and cessation of mare volcanism.

## CONCLUSIONS

We have considered a number of simple analytical representations of the rheological response of a planet to the surface load associated with the topography of a large impact basin. For features with horizontal dimensions in excess of the thickness of a lithosphere of high viscosity, both the decrease of effective viscosity with depth and the partial to complete isostatic compensation of topographic relief have a pronounced signature in the characteristic times for viscous relaxation. The effect of a decreasing viscosity with depth is to enhance the rate of viscous relaxation at long wavelengths. The effect of isostatic compensation of topographic relief is to decrease substantially the rate of relaxation of a fraction of long-wavelength topography, with that fraction dependent on the degree of initial compensation. The available gravity data indicate that the topographic relief of young lunar basins was at least 50 to 60% compensated by crustal thickness variations prior to any mare basalt fill, so that this compensation must be taken into account in modeling viscous relaxation of basin-scale features.

The topographic relief of the pre-Nectarian Tranquillitatis basin on the central nearside of the moon, after removing the effect of mare basalt fill on present topography, is consistent with significant viscous relaxation of relief prior to the oldest episode of mare volcanism preserved as a surface unit in the Tranquillitatis region. The derived value of the quantity  $t/\eta$ , where  $t$  is the time interval over which significant viscous relaxation occurred and  $\eta$  is the effective viscosity of the lunar crust during that time, is within the range of values determined by Hall *et al.* [1981] from topographic profiles of large (16- to 40-km diameter) floor-fractured craters on the lunar nearside.

The large topographic relief indicated by laser altimeter data for the 2000-km-diameter South Pole–Aitken basin on the lunar farside is inconsistent with significant viscous relaxation of that basin. Since that farside basin is both older and larger than nearside basins such as Tranquillitatis which have substantially modified topographic profiles, the effective viscosity of the farside crust must have been at least an order of magnitude larger than that of the nearside crust between about 3.8 and perhaps 4 b.y. ago. The most likely cause of this difference is a lower mean crustal temperature on the farside during that time. Lower crustal temperatures on the lunar farside than the nearside may have dated from the processes of crust-mantle differentiation that led to the offset of lunar centers and to the asymmetry in surface concentrations of radioactive elements. The duration of such a temperature difference would have been substantially augmented by the larger amount of nearside heating associated with impact basin formation during the terminal phases of heavy bombardment as well as by the greater amount of heating on the nearside associated with mare volcanism.

## APPENDIX: RELAXATION OF A HARMONIC TOPOGRAPHIC LOAD ON A VISCOUS LAYER OVERLYING AN INVISCID HALF SPACE

Consider a viscous, incompressible layer of thickness  $H$  overlying an inviscid fluid half space. Let  $\eta$  be the viscosity of the layer and let  $\rho$  and  $\rho_m$  be the density of the layer and of the half space, respectively. Let the topography at the surface and at the base of the layer be two dimensional:  $z =$

$\zeta(x, t)$  and  $z = H + \varepsilon(x, t)$ , respectively, where  $x$  is the horizontal coordinate,  $z$  is the vertical coordinate (positive downwards), and  $t$  is time (see Figure A1). Let  $\zeta$  and  $\varepsilon$  be harmonic in  $x$  at time  $t = 0$ :

$$\begin{aligned} \zeta(x, 0) &= \zeta_0 \cos kx \\ \varepsilon(x, 0) &= \varepsilon_0 \cos kx \end{aligned} \tag{A1}$$

where  $k$  is the horizontal wave number.

We seek solutions for  $\zeta$  and  $\varepsilon$  of the form

$$\begin{aligned} \zeta(x, t) &= F(t) \cos kx & F(0) &= \zeta_0 \\ \varepsilon(x, t) &= G(t) \cos kx & G(0) &= \varepsilon_0 \end{aligned} \tag{A2}$$

The quantities  $\varepsilon_0$  and  $\zeta_0$  may be directly related by isostatic compensation prior to viscous relaxation. For local isostasy, the degree of isostatic compensation  $c$  ( $0 \leq c \leq 1$ ) is given by

$$c = -\Delta\rho \varepsilon_0 / \rho \zeta_0 \tag{A3}$$

where  $\Delta\rho = \rho_m - \rho$ .

We assume that the viscous layer at  $t > 0$  is always in a state of quasi-static equilibrium, so that the statement of momentum conservation is

$$\sigma_{ij} + f_i = 0 \quad i, j = 1, 2, 3 \tag{A4}$$

where  $\sigma_{ij}$  is a component of the stress tensor (positive in tension),  $f_i$  is a component of the body force,  $(1, 2, 3) = (x, y, z)$ , the comma before the subscript denotes differentiation with respect to the subscripted coordinate, and repeated indices imply summation. In this problem,  $f_x = f_y = 0$  and  $f_z = \rho g$ . The stress tensor is given by [e.g., Fung, 1977]

$$\sigma_{ij} = -p\delta_{ij} + 2\eta V_{ij} \tag{A5}$$

where  $p$  is the pressure,  $\delta_{ij}$  is the Kronecker delta, and

$$V_{ij} = \frac{1}{2} \left( \frac{\partial v_i}{\partial x_j} + \frac{\partial v_j}{\partial x_i} \right) \tag{A6}$$

where  $v_i$  is a component of fluid velocity. Because the problem is two-dimensional,  $v_y = 0$  and  $\partial/\partial y = 0$ . Then the condition of incompressibility,  $v_{kk} = 0$ , is satisfied by

$$\begin{aligned} v_x &= -\partial\psi/\partial z \\ v_z &= \partial\psi/\partial x \end{aligned} \tag{A7}$$

where  $\psi$  is a scalar stream function. From (A4)–(A7) we have the field equations

$$\begin{aligned} -\frac{\partial p}{\partial x} - \eta \left( \frac{\partial^3 \psi}{\partial x^2 \partial z} + \frac{\partial^3 \psi}{\partial z^3} \right) &= 0 \\ -\frac{\partial p}{\partial z} + \eta \left( \frac{\partial^3 \psi}{\partial x^3} + \frac{\partial^3 \psi}{\partial x \partial z^2} \right) + \rho g &= 0 \end{aligned} \tag{A8}$$

There are six boundary conditions that must be specified to determine a solution to (A8). Two kinematic boundary conditions on  $v_z(x, z, t)$  are

$$\begin{aligned} v_z(x, \zeta, t) &= \dot{\zeta}(x, t) \\ v_z(x, H + \varepsilon, t) &= \dot{\varepsilon}(x, t) \end{aligned} \tag{A9}$$

where the dot denotes  $\partial/\partial t$ . In addition there are four stress boundary conditions: the tangential component of stress must vanish at both the top and bottom of the viscous layer,

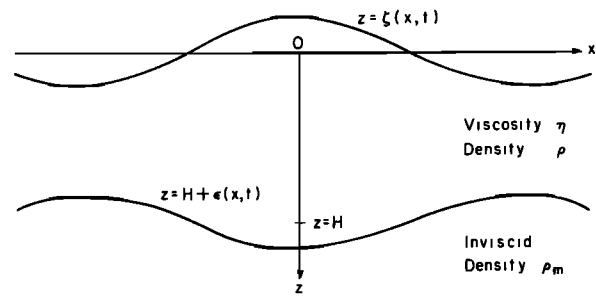


Fig. A1. Schematic view of viscous relaxation problem for a viscous layer over an inviscid half space of higher density. Parameters are defined in the text.

and the normal component of stress must be zero at the surface and  $-\rho g H - \rho_m g \varepsilon(x, t)$  at the interface, where  $g$  is gravitational acceleration. The condition at the interface reflects the hydrostatic state of the inviscid substratum. Note that these boundary conditions differ from those assumed by Ramberg [1968] in his treatment of this problem. We assume that the solutions to (A8) are of the form

$$\begin{aligned} p(x, z, t) &= \rho g z + P(z, t) \cos kx \\ \psi(x, z, t) &= \Psi(z, t) \sin kx \end{aligned} \tag{A10}$$

Substitution of (A10) into (A8) gives

$$\begin{aligned} P &= -k\eta \frac{\partial \Psi}{\partial z} + \frac{\eta}{k} \frac{\partial^3 \Psi}{\partial z^3} \\ \frac{\partial^4 \Psi}{\partial z^4} - 2k^2 \frac{\partial^2 \Psi}{\partial z^2} + k^4 \Psi &= 0 \end{aligned} \tag{A11}$$

Equations (A11) have the solutions

$$\begin{aligned} \Psi(z, t) &= \frac{\rho g}{2\eta k^3} [A(t)e^{-kz} + B(t)kze^{-kz} + C(t)e^{kz} + D(t)kze^{kz}] \\ P(z, t) &= \frac{\rho g}{k} [B(t)e^{-kz} + D(t)e^{kz}] \end{aligned} \tag{A12}$$

where  $A, B, C,$  and  $D$  are dimensionless functions of time. Substitution of (A12) into (A10) gives

$$\begin{aligned} p(x, z, t) &= \rho g z + \frac{\rho g}{k} [B(t)e^{-kz} + D(t)e^{kz}] \cos kx \\ \psi(x, z, t) &= \frac{\rho g}{2\eta k^3} [A(t)e^{-kz} + B(t)kze^{-kz} + C(t)e^{kz} \\ &\quad + D(t)kze^{kz}] \sin kx \end{aligned} \tag{A13}$$

and the vertical velocity and stress components are given by

$$\begin{aligned} v_z &= \frac{\rho g}{2\eta k^2} [Ae^{-kz} + Bkze^{-kz} + Ce^{kz} + Dkze^{kz}] \cos kx \\ \sigma_{xz} &= -\frac{\rho g}{k} [(A - B)e^{-kz} + Bkze^{-kz} + (C + D)e^{kz} \\ &\quad + Dkze^{kz}] \sin kx \end{aligned} \tag{A14}$$

$$\sigma_{zz} = \frac{\rho g}{k} [-kz + (-Ae^{-kz} - Bkze^{-kz} + Ce^{kz} + Dkze^{kz}) \cos kx]$$

Application of the boundary conditions, which allows us to solve for  $A, B, C,$  and  $D,$  requires some care. Strictly, the six boundary conditions must be applied at  $z = \zeta(x, t)$  and  $z = H + \varepsilon(x, t),$  and the tangential and normal components of stress on these surfaces are each linear combinations of  $\sigma_{xz}$  and  $\sigma_{zz}.$  Using the exact boundary conditions yields a system of nonlinear equations in  $A, B, C, D, F,$  and  $G.$  To linearize the equations for  $F$  and  $G,$  we make two simplifying assumptions:

1. We assume that

$$k|F| \ll 1 \quad k|G| \ll 1 \tag{A15}$$

This is equivalent to assuming that the topography at the top and bottom of the layer is gentle.

2. We further assume that the magnitudes of  $A, B, C,$  and  $D$  are small in comparison to unity; the implications of this assumption are discussed further below after solutions are obtained for these quantities.

With assumption 1, the boundary conditions on stress become

$$\begin{aligned} \sigma_{xz}(x, \zeta, t) &= 0 \\ \sigma_{xz}(x, H + \varepsilon, t) &= 0 \\ \sigma_{zz}(x, \zeta, t) &= 0 \end{aligned} \tag{A16}$$

$$\sigma_{zz}(x, H + \varepsilon, t) = -\rho g H - \rho_m g \varepsilon(x, t)$$

With assumptions 1 and 2 together, we may ignore variations of  $z$  at the top and bottom of the layer for all terms in the boundary conditions on  $v_z, \sigma_{xz},$  and  $\sigma_{zz}$  except for the term  $-\rho g z$  in  $\sigma_{zz},$  where the variations described by  $\zeta$  and  $\varepsilon$  must be retained. The results that follow are then valid to first order in the small quantities  $A, B, C, D, kF,$  and  $kG.$

From the kinematic boundary condition (A9), with (A2) and (A14), we have

$$\dot{F}(t) = \frac{\rho g}{2\eta k^2} [A(t) + C(t)] \tag{A17}$$

$$\dot{G}(t) = \frac{\rho g}{2\eta k^2} [A(t)e^{-kH} + B(t)kHe^{-kH} + C(t)e^{kH} + D(t)kHe^{kH}]$$

From the conditions on shear stress in (A16), together with (A14), we have

$$A(t) - B(t) + C(t) + D(t) = 0$$

$$A(t)e^{-kH} + B(t)[kH - 1]e^{-kH} + C(t)e^{kH} + D(t)[kH + 1]e^{kH} = 0 \tag{A18}$$

From the boundary conditions on normal stress in (A16), with (A14), we have

$$-kF(t) - A(t) + C(t) = 0$$

$$\begin{aligned} \frac{\Delta \rho}{\rho} kG(t) - A(t)e^{-kH} - B(t)kHe^{-kH} + C(t)e^{kH} \\ + D(t)kHe^{kH} = 0 \end{aligned} \tag{A19}$$

We may solve (A18) and (A19) for  $A, B, C,$  and  $D$  in terms of  $F$  and  $G.$  We then substitute these expressions into (A17). After some algebra, we obtain

$$\begin{aligned} \dot{F}(t) &= \frac{\rho g}{2\eta k} \frac{[e^{-2kH} - 4kH - e^{2kH}]}{E} F(t) \\ &+ \frac{\Delta \rho g}{2\eta k} \frac{[2(1 - kH)e^{-kH} - 2(1 + kH)e^{kH}]}{E} G(t) \end{aligned} \tag{A20}$$

$$\begin{aligned} \dot{G}(t) &= \frac{\rho g}{2\eta k} \frac{[2(1 - kH)e^{-kH} - 2(1 + kH)e^{kH}]}{E} F(t) \\ &+ \frac{\Delta \rho g}{2\eta k} \frac{[e^{-2kH} - 4kH - e^{2kH}]}{E} G(t) \end{aligned}$$

where

$$E = e^{-2kH} + e^{2kH} - 4(kH)^2 - 2$$

As a necessary step in the solution (A20), we also obtain expressions for the quantities  $A, B, C,$  and  $D,$  which we had previously assumed to satisfy

$$|A|, |B|, |C|, |D| \ll 1 \tag{A21}$$

These expressions are

$$\begin{aligned} A(t)E &= kF[2(kH)^2 - 2kH + 1 - e^{2kH}] \\ &+ \frac{\Delta \rho}{\rho} kG[-(kH - 1)e^{-kH} - (kH + 1)e^{kH}] \end{aligned}$$

$$\begin{aligned} B(t)E &= kF[1 - 2kH - e^{2kH}] + \frac{\Delta \rho}{\rho} kG[e^{-kH} \\ &- (2kH + 1)e^{kH}] \end{aligned}$$

$$C(t) = A + kF$$

$$D(t) = B - 2A - kF$$

At short wavelengths ( $kH \rightarrow \infty$ ),  $A$  and  $B$  are of order  $kF$  and  $C$  and  $D$  vanish; thus (A15) is a sufficient condition for the assumption (A21). In the limit of long wavelengths ( $kH \rightarrow 0$ ), the magnitudes of  $A, B, C,$  and  $D$  are all equal to

$$\frac{3}{(kH)^3} \left( kF + \frac{\Delta \rho}{\rho} kG \right)$$

The assumption (A21) is thus valid for small  $k$  only if

$$\left| kF + \frac{\Delta \rho}{\rho} kG \right| \ll (kH)^3/3 \tag{A22}$$

Note that the quantity on the left-hand side of the inequality is identically zero in the case of complete isostatic compensation.

The solution to the coupled differential equations (A20) is of the form

$$\begin{aligned} F(t) &= F_1 e^{-t/\tau_1} + F_2 e^{-t/\tau_2} \\ G(t) &= G_1 e^{-t/\tau_1} + G_2 e^{-t/\tau_2} \end{aligned} \tag{A23}$$

where  $\tau_1$  and  $\tau_2$  are time constants related to the eigenvalues  $\lambda_1$  and  $\lambda_2$  of the matrix of coefficients of  $F(t)$  and  $G(t)$  in

(A20) by  $\tau_1 = -1/\lambda_1$ ,  $\tau_2 = -1/\lambda_2$ , and where  $F_1$ ,  $F_2$ ,  $G_1$ , and  $G_2$  are found by eigenvector analysis. If we define

$$\alpha = \frac{g}{2\eta k} \frac{e^{-2kH} - 4kH - e^{2kH}}{E} \quad (A24)$$

$$\beta = \frac{g}{2\eta k} \frac{2(1 - kH)e^{-kH} - 2(1 + kH)e^{kH}}{E}$$

then (A20) becomes

$$\begin{aligned} \dot{F}(t) &= \alpha \rho F(t) + \beta \Delta \rho G(t) \\ \dot{G}(t) &= \beta \rho F(t) + \alpha \Delta \rho G(t) \end{aligned} \quad (A25)$$

which has eigenvalues

$$\begin{aligned} \lambda_1, \lambda_2 &= \frac{\alpha}{2}(\rho + \Delta \rho) \pm \frac{1}{2}[\alpha^2(\rho + \Delta \rho)^2 + 4(\beta^2 - \alpha^2)\rho\Delta\rho]^{1/2} \\ &= -\frac{1}{\tau_1}, -\frac{1}{\tau_2} \end{aligned} \quad (A26)$$

and the solution

$$\begin{aligned} F(t) &= [(\alpha\rho - \lambda_2)F(0) + \beta\Delta\rho G(0)] \frac{e^{\lambda_1 t}}{\lambda_1 - \lambda_2} \\ &\quad + [(\lambda_1 - \alpha\rho)F(0) - \beta\Delta\rho G(0)] \frac{e^{\lambda_2 t}}{\lambda_1 - \lambda_2} \\ G(t) &= [\beta\rho F(0) + (\lambda_1 - \alpha\rho)G(0)] \frac{e^{\lambda_1 t}}{\lambda_1 - \lambda_2} \\ &\quad + [-\beta\rho F(0) + (\alpha\rho - \lambda_2)G(0)] \frac{e^{\lambda_2 t}}{\lambda_1 - \lambda_2} \end{aligned} \quad (A27)$$

The combination of (A27), (A24), and (A2) completes the solution.

Some special cases are of interest. Consider first the case  $\Delta\rho = 0$ ; i.e., no density contrast at  $z = H$ . Then the two equations in (A25) decouple, and

$$\dot{F}(t) = \alpha \rho F(t)$$

which has the solution

$$F(t) = F(0)e^{-t/\tau}$$

where

$$\tau = -\frac{1}{\alpha\rho} = \frac{2\eta k}{\rho g} \left[ \frac{e^{2kH} + e^{-2kH} - 4(kH)^2 - 2}{e^{2kH} - e^{-2kH} + 4kH} \right] \quad (A28)$$

In the limiting case  $kH \rightarrow \infty$ ,

$$\tau \rightarrow 2\eta k/\rho g$$

or the half-space solution. In the limiting case  $kH \rightarrow 0$ ,

$$\tau \rightarrow \frac{2\eta k}{\rho g} \frac{(kH)^3}{6} \quad (A29)$$

With a nonzero density contrast at  $z = H$ , there are, in general, two time constants to the viscous relaxation prob-

lem. In the limiting case  $kH \rightarrow \infty$ ,

$$\begin{aligned} \tau_1 &= -1/\lambda_1 \rightarrow 2\eta k/\Delta\rho g \\ \tau_2 &= -1/\lambda_2 \rightarrow 2\eta k/\rho g \end{aligned} \quad (A30)$$

and

$$\begin{aligned} F_1 &= 0 & F_2 &= F(0) \\ G_1 &= G(0) & G_2 &= 0 \end{aligned} \quad (A31)$$

Thus in this short-wavelength limit, following (A23),

$$\begin{aligned} F(t) &= F(0)e^{-\rho g t/2\eta k} \\ G(t) &= G(0)e^{-\Delta\rho g t/2\eta k} \end{aligned} \quad (A32)$$

so that relaxation on the two interfaces is decoupled, with surface topography relaxing according to the half-space solution and topography at the density interface relaxing at a slower rate corresponding to the solution for the decay of relief on the interface between two adjoining half spaces, a viscous one overlying an inviscid one, with a density constant  $\Delta\rho$  in a uniform gravitational field.

In the limiting case  $kH \rightarrow 0$ ,

$$\begin{aligned} \tau_1 &\rightarrow \frac{4\eta}{H} \frac{\rho_m}{g \rho \Delta\rho} \\ \tau_2 &\rightarrow \frac{2\eta k}{\rho_m g} \frac{(kH)^3}{6} \end{aligned} \quad (A33)$$

so that  $\tau_1$  is independent of  $k$  and  $\tau_2$  is similar to  $\tau$  in (A29) with  $\rho_m$  replacing  $\rho$  as the density of the half space. Assuming partial to complete compensation of initial topography,

$$\begin{aligned} F_1 &= \left( \frac{\Delta\rho + c\rho}{\rho_m} \right) F(0) = \frac{\Delta\rho}{\rho_m} [F(0) - G(0)] \\ F_2 &= \frac{\rho}{\rho_m} (1 - c) F(0) \end{aligned} \quad (A34)$$

$$G_1 = \frac{-\rho}{\rho_m} \left( \frac{\Delta\rho + c\rho}{\Delta\rho} \right) F(0) = \frac{\rho}{\rho_m} [G(0) - F(0)]$$

$$G_2 = \frac{\rho}{\rho_m} (1 - c) F(0)$$

Thus in this long-wavelength limit we may write

$$\begin{aligned} F(t) &= \frac{\Delta\rho}{\rho_m} [F(0) - G(0)]e^{-t/\tau_1} + \frac{\rho}{\rho_m} (1 - c)F(0)e^{-t/\tau_2} \\ G(t) &= \frac{\rho}{\rho_m} [G(0) - F(0)]e^{-t/\tau_1} + \frac{\rho}{\rho_m} (1 - c)F(0)e^{-t/\tau_2} \end{aligned} \quad (A35)$$

The two second terms in the right-hand side of (A35) are identical, so that at short time scales governed by  $\tau_2 \sim k^4$  there is (for  $c < 1$ ) a rapid partial relaxation of surface topography and a completely parallel movement of the density interface. The two first terms in the right-hand side of (A35) decay at the much longer time constant  $\tau_1$ . The coefficients of the  $e^{-t/\tau_1}$  terms for  $F$  and  $G$  are in the ratio  $-\Delta\rho/\rho$ , so they correspond to complete Airy isostatic compensation. Thus in this long-wavelength limit, an initially

isostatic topography will remain isostatically compensated for all  $t > 0$ , and an initial topography only partially compensated ( $c < 1$ ) will become completely compensated for  $t \gg \tau_2$ .

**Acknowledgments.** We thank Dorothy Frank and Jan Nattier-Barbaro for their assistance in the preparation of this manuscript, Suzanne Church for help in the preparation of figures, and Roger Phillips and Bill McKinnon for constructive reviews of our arguments. The research reported here was supported by the NASA Planetary Geology and Planetary Geophysics and Geochemistry programs under grants NSG-7081 and NSG-7297 at MIT and grant 40-002-116 at Brown University. One of us (SCS) also gratefully acknowledges the support of an Alfred P. Sloan Research Fellowship.

#### REFERENCES

- Abramowitz, M., and I. A. Stegun, *Handbook of Mathematical Functions, Appl. Math. Ser.*, vol. 55, 1046 pp., National Bureau Standards, Washington, D. C., 1964.
- Avé Lallemant, H. G., Experimental deformation of diopside and websterite, *Tectonophysics*, **48**, 1-28, 1978.
- Baldwin, R. B., Rille pattern in the lunar crater Humboldt, *J. Geophys. Res.*, **73**, 3227-3229, 1968.
- Baldwin, R. B., The question of isostasy on the moon, *Phys. Earth Planet. Inter.*, **4**, 167-179, 1971.
- Bowin, C., B. Simon, and W. R. Wollenhaupt, Mascons: A two-body solution, *J. Geophys. Res.*, **80**, 4947-4955, 1975.
- Boyce, J. M., Ages of flow units in the lunar nearside maria based on Lunar Orbiter IV photographs, *Proc. Lunar Sci. Conf.*, **7th**, 2717-2728, 1976.
- Bratt, S. R., S. C. Solomon, and J. W. Head, The evolution of multi-ringed basins: Cooling, subsidence and thermal stress (abstract), *Lunar Planet. Sci.*, **12**, 109-111, 1981.
- Cadogan, P. H., Oldest and largest lunar basin?, *Nature*, **250**, 315-316, 1974.
- Cathles, L. M., *The Viscosity of the Earth's Mantle*, 386 pp., Princeton University Press, Princeton, N. J., 1975.
- Church, S., J. W. Head, and S. C. Solomon, Multi-ringed basin interiors: Structure and early evolution of Orientale (abstract), *Lunar Planet. Sci.*, **13**, 98-99, 1982.
- Comer, R. P., S. C. Solomon and J. W. Head, Elastic lithosphere thickness on the moon from mare tectonic features: A formal inversion, *Proc. Lunar Planet. Sci. Conf.*, **10th**, 2441-2463, 1979.
- Comer, R. P., S. C. Solomon, and J. W. Head, Thickness of the Martian lithosphere beneath volcanic loads: A consideration of time dependent effects (abstract), *Lunar Planet. Sci.*, **11**, 171-173, 1980.
- Daneš, Z. F., Rebound processes in large craters, in *Astrogeologic Studies*, annual progress report, pt. A, pp. 81-100, U.S. Geological Survey, Reston, Va., 1965.
- DeHon, R. A., Thickness of mare material in the Tranquillitatis and Nectaris basins, *Proc. Lunar Sci. Conf.*, **5th**, 53-59, 1974.
- DeHon, R. A., and J. D. Waskom, Geologic structure of the eastern mare basins, *Proc. Lunar Sci. Conf.*, **7th**, 2729-2746, 1976.
- Dvorak, J., and R. J. Phillips, Isostatic compensation with density stratification (abstract), *Eos Trans. AGU*, **56**, 1012, 1975.
- Dvorak, J., and R. J. Phillips, Lunar Bouguer gravity anomalies: Imbrian age craters, *Proc. Lunar Planet. Sci. Conf.*, **9th**, 3651-3668, 1978.
- Dvorak, J., and R. J. Phillips, Gravity anomaly and structure associated with the Lamont region of the moon, *Proc. Lunar Planet. Sci. Conf.*, **10th**, 2265-2275, 1979.
- Ferrari, A. J., D. L. Nelson, W. L. Sjogren, and R. J. Phillips, The isostatic state of the lunar Apennines and regional surroundings, *J. Geophys. Res.*, **83**, 2863-2871, 1978.
- Fung, Y. C., *A First Course in Continuum Mechanics*, 340 pp., Prentice-Hall, Englewood Cliffs, N. J., 1977.
- Goetze, C., The mechanics of creep in olivine, *Philos. Trans. R. Soc. London, Ser. A*, **288**, 99-119, 1978.
- Hall, J. L., S. C. Solomon, and J. W. Head, Lunar floor-fractured craters: Evidence for viscous relaxation of crater topography, *J. Geophys. Res.*, **86**, 9537-9552, 1981.
- Hartmann, W. K., and C. A. Wood, Moon: Origin and evolution of multi-ring basins, *Moon*, **3**, 3-78, 1971.
- Head, J. W., Orientale multi-ringed basin interior and implications for the petrogenesis of lunar highland samples, *Moon*, **11**, 327-356, 1974.
- Head, J. W., Some geologic observations concerning lunar geophysical models, The Soviet-American Conference on Cosmochemistry of the Moon and Planets, edited by J. H. Pomeroy and N. J. Hubbard, *NASA Spec. Publ.*, **SP-370**, 407-416, 1977.
- Head, J. W., and S. C. Solomon, Lunar basin structures: Possible influence of variations in lithospheric thickness (abstract), *Lunar Planet. Sci.*, **11**, 421-423, 1980.
- Head, J. W., and S. C. Solomon, Impact basins: Stages in basin formation and evolution (abstract), *Lunar Planet. Sci.*, **12**, 424-426, 1981.
- Head, J. W., E. Robinson, and R. J. Phillips, Topography of the Orientale basin (abstract), *Lunar Planet. Sci.*, **12**, 421-423, 1981.
- Howard, K. A., D. E. Wilhelms, and D. H. Scott, Lunar basin formation and highland stratigraphy, *Rev. Geophys. Space Phys.*, **12**, 309-327, 1974.
- Kaula, W. M., G. Schubert, R. E. Lingenfelter, W. L. Sjogren, and W. R. Wollenhaupt, Lunar topography from Apollo 15 and 16 laser altimetry, *Proc. Lunar Sci. Conf.*, **4th**, 2811-2819, 1973.
- Kaula, W. M., G. Schubert, R. E. Lingenfelter, W. L. Sjogren, and W. R. Wollenhaupt, Apollo laser altimetry and inferences as to lunar structure, *Proc. Lunar Sci. Conf.*, **5th**, 3049-3058, 1974.
- Koyama, J., and Y. Nakamura, Re-examination of the lunar seismic velocity structure based on the complete data set (abstract), *Lunar Planet. Sci.*, **10**, 685-687, 1979.
- Kuiper, G. P., R. G. Strom, E. A. Whitaker, J. W. Fountain, and S. M. Larson, Consolidated Lunar Atlas, *Contrib. 4*, Lunar and Planet. Lab., Univ. of Ariz., Tucson, 1967.
- Kunze, A. W. G., Creep response of the lunar crust in mare regions from an analysis of crater deformation, *Phys. Earth Planet. Inter.*, **8**, 375-387, 1974.
- Malin, M. C., Comparison of large crater and multiringed basin populations on Mars, Mercury and the Moon, *Proc. Lunar Sci. Conf.*, **7th**, 3589-3602, 1976.
- Masursky, H., A preliminary report on the role of isostatic rebound in the geologic development of the lunar crater Ptolemaeus, in *Astrogeologic Studies*, annual progress report, pt. A, pp. 102-134, U.S. Geological Survey, Reston, Va., 1964.
- Masursky, H., E. Eliason, P. G. Ford, G. E. McGill, G. H. Pettengill, G. G. Schaber, and G. Schubert, Pioneer Venus radar results: Geology from images and altimetry, *J. Geophys. Res.*, **85**, 8232-8260, 1980.
- McGetchin, T. R., M. Settle, and J. W. Head, Radial thickness variation in impact crater ejecta: Implications for lunar basin deposits, *Earth Planet. Sci. Lett.*, **20**, 226-236, 1973.
- McKinnon, W. B., and H. J. Melosh, Evolution of planetary lithospheres: Evidence from multiringed structures on Ganymede and Callisto, *Icarus*, **44**, 454-471, 1980.
- Melosh, H. J., and W. B. McKinnon, The mechanics of ringed basin formation, *Geophys. Res. Lett.*, **5**, 985-988, 1978.
- Moore, H. J., C. A. Hodges, and D. H. Scott, Multi-ringed basins—Illustrated by Orientale and associated features, *Proc. Lunar Sci. Conf.*, **5th**, 71-100, 1974.
- Morris, E. C., and D. E. Wilhelms, Geologic map of the Julius Caesar Quadrangle of the moon, *Geol. Atlas Moon, Map I-510*, U.S. Geological Survey, Reston, Va., 1967.
- O'Keefe, J. D., and T. J. Ahrens, Impact-induced energy partitioning, melting, and vaporization on terrestrial planets, *Proc. Lunar Sci. Conf.*, **8th**, 3357-3374, 1977.
- Parmentier, E. M., and J. W. Head, Viscous relaxation of impact craters on icy planetary surfaces: Determination of viscosity variations with depth, *Icarus*, **47**, 100-111, 1981.
- Phillips, R. J., and J. Dvorak, The origin of lunar mascons: Analysis of the Bouguer gravity associated with Grimaldi, Multi-Ring Basins, *Proc. Lunar Planet. Sci.*, **12A**, 91-104, 1981.
- Phillips, R. J., and K. Lambeck, Gravity fields of the terrestrial planets—Long wavelength anomalies and tectonics, *Rev. Geophys. Space Phys.*, **18**, 27-76, 1980.
- Pike, R. J., Meteoritic origin and consequent endogenic modification of large lunar craters—A study in analytical geomorphology, Ph. D. thesis, 404 p., Univ. of Mich., Ann Arbor, 1968.
- Pike, R. J., Geometric interpretation of lunar craters, *U.S. Geol. Surv. Prof. Pap.*, **1046-C**, 77 pp., 1980.
- Ramberg, H., Fluid dynamics of layered systems in the field of

- gravity, a theoretical basis for certain global structures and isostatic adjustment, *Phys. Earth Planet. Inter.*, *1*, 63–87, 1968.
- Schaber, G. G., and J. M. Boyce, Probable distribution of large impact basins on Venus: Comparison with Mercury and the Moon, in *Impact and Explosion Cratering*, edited by D. J. Rody, R. O. Pepin, and R. B. Merrill, pp. 603–612, Pergamon, Elmsford, N.Y., 1977.
- Schaber, G. G., J. M. Boyce, and N. J. Trask, Moon-Mercury: Large impact structures, isostasy and average crustal viscosity, *Phys. Earth Planet. Inter.*, *15*, 189–201, 1977.
- Schirmerman, L. A. (Ed.), *Lunar Cartographic Dossier*, Defense Mapping Agency Aerospace Center, St. Louis, Mo., 1973.
- Schultz, P. H., Floor-fractured lunar craters, *Moon*, *15*, 241–273, 1976.
- Scott, D. H., J. M. Diaz, and J. A. Watkins, The geologic evaluation and regional synthesis of metric and panoramic photographs, *Proc. Lunar Sci. Conf.*, *6th*, 2531–2540, 1975.
- Scott, R. F., Viscous flow of craters, *Icarus*, *7*, 139–148, 1967.
- Sjogren, W. L., and J. C. Smith, Quantitative mass distribution models for Mare Orientale, *Proc. Lunar Sci. Conf.*, *7th*, 2639–2648, 1976.
- Smith, B. A., L. A. Soderblom, T. V. Johnson, A. P. Ingersoll, S. A. Collins, E. M. Shoemaker, G. E. Hunt, H. Masursky, M. H. Carr, M. E. Davies, A. F. Cook II, J. Boyce, G. E. Danielson, T. Owen, C. Sagan, R. F. Beebe, J. Veverka, R. G. Strom, J. F. McCauley, D. Morrison, G. A. Briggs, and V. E. Suomi, The Jupiter system through the eyes of Voyager 1, *Science*, *204*, 951–972, 1979.
- Solomon, S. C., The nature of isostasy on the Moon: How big a Pratt-fall for Airy models?, *Proc. Lunar Planet. Sci. Conf.*, *9th*, 3499–3511, 1978.
- Solomon, S. C., and J. W. Head, Vertical movement in mare basins: Relation to mare emplacement, basin tectonics, and lunar thermal history, *J. Geophys. Res.*, *84*, 1667–1682, 1979.
- Solomon, S. C., and J. W. Head, Lunar mascon basins: Lava filling, tectonics, and evolution of the lithosphere, *Rev. Geophys. Space Phys.*, *18*, 107–141, 1980.
- Solomon, S. C., J. W. Head, and R. P. Comer, Thickness of the Martian lithosphere from tectonic features: Evidence for lithospheric thinning beneath volcanic provinces (abstract), Reports of Planetary Geology Program, 1978–1979, *NASA Tech. Memo.*, *80339*, 60–62, 1979.
- Solomon, S. C., T. J. Ahrens, P. Cassen, A. T. Hsui, J. W. Minear, R. T. Reynolds, N. H. Sleep, D. W. Strangway, and D. L. Turcotte, Thermal histories of the terrestrial planets, in *Basaltic Volcanism on the Terrestrial Planets*, pp. 1129–1234, Pergamon, Elmsford, N.Y., 1981.
- Stevenson, D. J., Lunar asymmetry and paleomagnetism, *Nature*, *287*, 520–521, 1980.
- Stuart-Alexander, D. E., Geologic map of the central far side of the moon, map I-1047, U.S. Geological Survey, Reston, Va., 1978.
- Stuart-Alexander, D. E., and K. A. Howard, Lunar maria and circular basins—A review, *Icarus*, *12*, 440–456, 1970.
- Thurber, C. H., and S. C. Solomon, An assessment of crustal thickness variations on the lunar near side: Models, uncertainties, and implications for crustal differentiation, *Proc. Lunar Planet. Sci. Conf.*, *9th*, 3481–3497, 1978.
- Toksöz, M. N., A. M. Dainty, S. C. Solomon, and K. R. Anderson, Structure of the moon, *Rev. Geophys. Space Phys.*, *12*, 539–567, 1974.
- Trombka, J. I., J. R. Arnold, I. Adler, A. E. Metzger, and R. C. Reedy, Lunar elemental analysis obtained from the Apollo gamma-ray and X-ray remote sensing experiment, The Soviet-American Conference on Cosmochemistry of the Moon and Planets, edited by J. H. Pomeroy and N. J. Hubbard, *NASA Spec. Publ.*, *SP-370*, 153–182, 1977.
- Tullis, J. A., High temperature deformation of rocks and minerals, *Rev. Geophys. Space Phys.*, *17*, 1137–1154, 1979.
- Wasserburg, G. J., D. A. Papanastassiou, F. Tera, and J. C. Huneke, Outline of a lunar chronology, *Philos. Trans. R. Soc. London, Ser. A*, *258*, 7–22, 1977.
- Wasson, J. T., and P. H. Warren, Contribution of the mantle to the lunar asymmetry, *Icarus*, *44*, 752–771, 1980.
- Whitaker, E. A., The lunar Procellarum basin, Multi-Ring Basins, *Proc. Lunar Planet. Sci.*, *12A*, 105–111, 1981.
- Wilhelms, D. E., Relative ages of lunar basins (abstract), *Reports of Planetary Geology Program, 1978–1979*, NASA Technical Memorandum 80339, 135–137, 1979.
- Wilhelms, D. E., Relative ages of lunar basins (II); Serenitatis (abstract), in *Reports of Planetary Geology Program—1981*, NASA Technical Memorandum 84211, 405–407, 1981.
- Wilhelms, D. E., and J. F. McCauley, Geologic map of the near side of the moon, map I-703, U.S. Geological Survey, Reston, Va., 1971.
- Wood, C. A., and A. W. Gifford, Evidence for the lunar big backside basin (abstract), in *Papers Presented to the Conference on Multi-Ring Basins: Formation and Evolution*, pp. 121–123, Lunar and Planetary Institute, Houston, Tex., 1980.
- Wood, C. A., and J. W. Head, Comparison of impact basins on Mercury, Mars and the moon, *Proc. Lunar Sci. Conf.*, *7th*, 3629–3651, 1976.

(Received September 22, 1981;  
revised January 26, 1982;  
accepted February 8, 1982.)